

AD _____

Award Number: W81XWH-04-1-0023

TITLE: MR Imaging Based Treatment Planning for Radiotherapy of Prostate Cancer

PRINCIPAL INVESTIGATOR: Lili Chen, Ph.D.

CONTRACTING ORGANIZATION: FOX Chase Cancer Center
Philadelphia PA 19111

REPORT DATE: February 2007

TYPE OF REPORT: Final

PREPARED FOR: U.S. Army Medical Research and Materiel Command
Fort Detrick, Maryland 21702-5012

DISTRIBUTION STATEMENT: Approved for Public Release;
Distribution Unlimited

The views, opinions and/or findings contained in this report are those of the author(s) and should not be construed as an official Department of the Army position, policy or decision unless so designated by other documentation.

REPORT DOCUMENTATION PAGE

Form Approved
OMB No. 0704-0188

Public reporting burden for this collection of information is estimated to average 1 hour per response, including the time for reviewing instructions, searching existing data sources, gathering and maintaining the data needed, and completing and reviewing this collection of information. Send comments regarding this burden estimate or any other aspect of this collection of information, including suggestions for reducing this burden to Department of Defense, Washington Headquarters Services, Directorate for Information Operations and Reports (0704-0188), 1215 Jefferson Davis Highway, Suite 1204, Arlington, VA 22202-4302. Respondents should be aware that notwithstanding any other provision of law, no person shall be subject to any penalty for failing to comply with a collection of information if it does not display a currently valid OMB control number. **PLEASE DO NOT RETURN YOUR FORM TO THE ABOVE ADDRESS.**

1. REPORT DATE (DD-MM-YYYY) 01-02-2007			2. REPORT TYPE Final		3. DATES COVERED (From - To) 01 Feb 04 – 31 Jan 07	
4. TITLE AND SUBTITLE MR Imaging Based Treatment Planning for Radiotherapy of Prostate Cancer					5a. CONTRACT NUMBER	
					5b. GRANT NUMBER W81XWH-04-1-0023	
					5c. PROGRAM ELEMENT NUMBER	
6. AUTHOR(S) Lili Chen, Ph.D. E-Mail: Lili.Chen@fcc.edu					5d. PROJECT NUMBER	
					5e. TASK NUMBER	
					5f. WORK UNIT NUMBER	
7. PERFORMING ORGANIZATION NAME(S) AND ADDRESS(ES) FOX Chase Cancer Center Philadelphia PA 19111					8. PERFORMING ORGANIZATION REPORT NUMBER	
9. SPONSORING / MONITORING AGENCY NAME(S) AND ADDRESS(ES) U.S. Army Medical Research and Materiel Command Fort Detrick, Maryland 21702-5012					10. SPONSOR/MONITOR'S ACRONYM(S)	
					11. SPONSOR/MONITOR'S REPORT NUMBER(S)	
12. DISTRIBUTION / AVAILABILITY STATEMENT Approved for Public Release; Distribution Unlimited						
13. SUPPLEMENTARY NOTES						
14. ABSTRACT This work is aimed at MRI-based treatment planning for radiation therapy. The tasks for the third year include (a) develop practical procedures for clinical implementation of MRI simulation; (b) develop guidelines for MRI-based treatment planning dose calculation, and (c) develop quality assurance programs for MRI simulation for prostate cancer treatment. We have developed a technique to create MR-based digitally reconstructed radiographs (DRR) for patient initial setup for clinical applications of MR-based treatment planning for prostate IMRT. The CT and MR images of twenty prostate patients were used for the study. The pelvic bony structures that are relevant for routine clinical patient setup were manually contoured on MRI. The contoured bony structures were assigned a bulk density of 2.0 g/cm ³ . The MRI based DRRs were generated. The accuracy of the MR based DRRs was quantitatively evaluated by comparing MR-based DRRs with CT-based DRRs for these patients. Our results showed that MR-based DRRs utilizing the outlines of relevant bony structures have an accuracy of about 3 mm, which is adequate for initial patient setup. This technique has been used, in combination with the BAT/in-room CT daily target localization techniques, for the clinical implementation of MRI-based treatment planning for prostate IMRT at FCCC.						
15. SUBJECT TERMS Radiotherapy, MRI treatment planning, Prostate Cancer, MRI-based DRRs						
16. SECURITY CLASSIFICATION OF:				17. LIMITATION OF ABSTRACT	18. NUMBER OF PAGES	19a. NAME OF RESPONSIBLE PERSON USAMRMC
a. REPORT U	b. ABSTRACT U	c. THIS PAGE U	19b. TELEPHONE NUMBER (include area code)			

Table of Contents

Front Cover 1

Standard Form 298 2

Table of Contents 3

Introduction 4

Body 4

Key Research Accomplishments 7

Reportable Outcomes 7

Conclusions 9

References 10

Appendices 10

Introduction

This project is aimed at exploring MR imaging based treatment planning for radiotherapy of prostate cancer. We have proposed to work on the third task for the third research year. The tasks include (1) develop practical procedures for clinical implementation of MRI simulation; (2) develop guidelines for MRI-based treatment planning dose calculation, and (3) develop quality assurance programs for MRI simulation for prostate cancer treatment. We describe our work for the third year as follows.

Body

In this annual report we report on the research accomplishments associated with the tasks outlined in the approved "Statement of Work" task 3 between Mar. 1, 2006 and Feb. 28, 2007. We will provide detailed information below for the results in the third year.

Task 3. Develop practical procedures for clinical implementation of MRI simulation

Creation of MR-based Digitally Reconstructed Radiographs (DRRs)

During this period, we have focused on developing a technique to create MR-based digitally reconstructed radiographs (DRR) for prostate IMRT patient setup when MR-based treatment planning is applied clinically. A paper entitled "MRI-Based Treatment Planning for Prostate IMRT: Creation of Digitally Reconstructed Radiographs (DRR)" has been accepted by *Int. J. Radiat. Oncol. Biol. Phys* (Chen et al 2007a). We studied MR image distortion corrections to further improve the accuracy of dose calculation for MR based treatment planning for prostate cancer. A paper entitled "Investigation of MR image distortion for radiotherapy treatment planning of prostate cancer" has been published in *Physics in Medicine and Biology* (Chen et al 2006). We also used the Monte Carlo method to further verify dosimetric accuracy and consistency for MR based IMRT treatment planning for prostate cancer. A short paper entitled "Monte Carlo dose verification of MR image based IMRT treatment planning for prostate cancer" has been submitted to XVth International Conference on the Use of Computers in Radiation Therapy (ICCR, Toronto, Jun 2007) (Chen et al 2007b). The two manuscripts together with the published paper are also attached to this report. We summarize the results and conclusions of these studies as follows.

Our previous studies demonstrated that MRI-based treatment planning meets the dosimetric accuracy for prostate IMRT and it is adequate to use unity density in treatment planning dose calculation with co-planar beam arrangements for prostate cancer treatment after correction of MRI distortions (Chen et al 2004a, 2004b). With CT-based treatment planning, the CT-based DRRs are routinely used for patient treatment set-up verification by comparing with portal film or electronic portal imaging devices (EPID). With MR-based treatment planning, Since MRI-derived DRRs do not provide enough bony structure information and therefore cannot be used directly for checking patient positions. To overcome this problem, we have developed a technique to create MR-based DRRs for patient initial setup for routine clinical applications of MR-based treatment planning for prostate patient treated with IMRT. Twenty prostate patients' CT and MR images were used for the study. CT and MR images were fused. The pelvic bony structures including femoral heads, pubic rami, ischium and ischial tuberosity that are relevant for routine clinical patient setup were manually contoured on axial MR images using the AcQsim planning system. The contoured bony structures were then assigned a bulk density of 2.0 g/cm^3 . The MRI based DRRs were generated. The accuracy of the MR based DRRs was quantitatively evaluated by comparing MR-based DRRs with CT-based DRRs for these patients. For each patient 8 measuring points on both coronal and sagittal DRRs were used for quantitative

evaluation. Our results showed that the maximum difference in the mean values of these measurement points is 1.3 and the maximum difference in absolute positions is within 3 mm for the 20 patients investigated. MR-based DRRs are comparable to CT-based DRRs for prostate IMRT. This technique has been used, in combination with the BAT/in-room CT daily target localization technique, for the clinical implementation of MRI-based treatment planning for prostate IMRT at FCCC.

Develop guidelines for MRI-based treatment planning dose calculation

We investigated the effect of MRI residual distortion after gradient distortion correction (GDC) on IMRT treatment planning and dosimetry accuracy. The residual distortion errors are less than 1 cm and will have negligible clinical impact for more than 90% of the prostate patients whose lateral dimensions are <40 cm. We have investigated on MR image distortion correction to further improve the accuracy of dose calculation for MR based treatment planning for prostate cancer. Our studies showed that, with our routine clinical 3-dimensional fast spin echo sequences (3DFSE, 256 x 256, 1.855 mm pixel, TR = 140 ms, TE = 3000 ms, BW readout gradient > 100 Hz/pixel), there was no patient-induced susceptibility distortions. Therefore, the residual machine specific geometrical distortions after the GDC could be quantified by phantom measurements and further reduced by our point-by-point correction technique. The effective field of view (FOV_{eff}) of the scanner was established based on the actual viewable areas with adequate geometric distortion corrections (ensuring < 5 mm distortion error). The effective FOV_{eff} for prostate imaging using a standard FOV of 48 cm has been expanded from 36 cm using the existing GDC software to 42 cm using the point-by-point distortion correction technique developed in this work. Our results indicated that, with the distortion maps established in this work, we could correct MR geometrical distortions for patients of lateral dimensions up to 42 cm. Significant improvement in dose calculation has been achieved based on a 1-2 cm improvement in patient external contour determination (Chen et al 2006).

Our previous study results showed that no clinically significant differences in dose calculations were found between MRI- and CT-based treatment plans using the same beam arrangements, dose constraints and optimization parameters. We also validated the dosimetry accuracy of MRI-based treatment planning by recomputing MRI-based IMRT plans using patient CT data and an IMRT QA phantom. The differences in dose distributions between MRI plans and the corresponding recomputed plans were generally within 3%/3mm. The differences in isocenter doses between MRI dose calculation and phantom measurements were within our clinical criterion of 4%.

This year we focused on the Monte Carlo method to further verify dosimetric accuracy and consistency for MR based IMRT treatment planning for prostate cancer. The Monte Carlo code used in this work was MCSIM, which is an EGS4/PRESTA user code developed at FCCC (Ma et al 2002). We have performed CT-based IMRT Monte Carlo dose calculations with and without heterogeneity corrections in order to investigate the heterogeneity effect caused by different beam angle arrangements. Based on the results, MR-based IMRT dose calculations were performed using either uniform density geometry or uniform density geometry with bulk electron density assigned to bony structures. For the plans with insignificant inhomogeneity effect, uniform geometries with water density were used in the MR-based dose calculation. For the plans that bony structure constitutes a large part of volume irradiated, uniform density geometry with bulk electron density assigned to bony structures was used in the MR-based dose calculation. Each IMRT plan was evaluated based on isodose distributions and dose volume histograms (DVHs) with CT-based or MR-based dose calculations. The clinical target volume (CTV) was chosen for the dose-volume comparison. Clinical quantities such as the mean dose, maximum and minimum dose received by the CTV and the critical structures were compared. The maximum dose

was defined as the highest dose received by 1% of the target volume and the minimum dose was defined as the lowest dose received by 99% of the target volume, respectively. Other parameters such as the dose at the isocenter and the dose received by 95% and 5% of the CTV were also compared. The paired CT and MR data for any patients in this work were pre-processed to have the same pixel resolution. The internal contours of the targets and critical organs were contoured by oncologists on the fused CT-MR images. A special computer code was developed to convert the patient CT and MR image data from the DICOM format to geometries specially formatted for the MCSIM code (Chen et al 2007).

Our results showed that the differences in dose calculations between CT data (with heterogeneity correction) and MR data (with uniform water equivalent geometry) were about 3% or less and less than 2% in the mean values for the 10 plans with beams arranged in the axial plane. For MR-based calculations (with homogeneous geometry), our results demonstrated that the differences between MR-based calculations and CT-based calculations (without heterogeneity correction) were less than 2% for the individual patients and about 1% in the mean values, which proved that MR-based IMRT plans can be used to replace CT-based planning clinically. The 1% - 2% differences in dose calculations were mainly caused by the setup uncertainties of the two imaging modalities if geometrical distortions on the MR images were corrected to less than 3 mm. For treatments in which relatively large amount of bones are irradiated, MR-based treatment planning with homogeneous geometry would not be appropriate because of the excessive attenuation of the photon beams passing through bony structures. However, by assigning bulk densities to the bony structures especially for the femurs and femoral heads, the dose differences could be reduced to less than 3%. The bulk density assigned to the femurs that gave the best fits to CT-based calculations with heterogeneity correction was 1.8g/cm^3 in our simulations (Chen et al 2007).

Develop quality assurance programs for MRI simulation for prostate cancer treatment

We have established a practical procedure for MR-based treatment planning. 1) An optimal MR protocol was first developed for contouring the target and critical structures. 2) We investigated the effect of MRI residual distortion after the GDC on IMRT treatment planning and dosimetry accuracy. The residual distortion errors are less than 1 cm and will have negligible clinical impact for more than 90% of the prostate patients whose lateral dimensions are <40 cm. For patients whose lateral dimensions are >40 cm we will use the point-by-point distortion correction technique developed in this work. Our results indicated that, with the distortion maps established in this work, we could correct MR geometrical distortions for patients of lateral dimensions up to 42 cm. 3) We have investigated optimal fiducial markers for MRI simulation. We have introduced a new donut-shaped marker to improve isocenter definition (IZI medical Product, Baltimore, Maryland 21244). The marker contains iodine with a 1.5 cm outer diameter and a 4 mm inner diameter. The centers of the markers can be detected clearly on one MR slice to define the treatment isocenter. To implement MRI simulation, a set of trackable lasers has been installed in the MR room for patient setup and isocenter determination. 4) We have demonstrated that MRI-based treatment planning meets the dosimetric accuracy for prostate IMRT and it is adequate to use unity density in treatment planning dose calculation with co-planar beams for prostate cancer treatment after MRI distortion corrections (Chen et al 2004a, 2004b), 5) We have developed practical methods for heterogeneity correction for MRI-based dose calculations (Chen et al 2007). 6) We will use existing Monte Carlo simulations as a quality assurance (QA) tool, implemented at FCCC, for IMRT dose verification using the EGS4/MCSIM Monte Carlo program (Ma et al 1999, 2000, 2002), in which a patient's CT and MLC leaf sequences

are directly used to reconstruct the dose to be received by the patient. We will MRI-scan IMRT QA phantoms and perform dose calculations to determine monitor units (MU) for IMRT plans and then compare with ion chamber measurements; 7) finally MRI-based DRRs are used during initial treatment setup together with CT-on-rails/cone-beam CT//BAT and later on as a backup for these imaging systems if the systems are down.

Key Research Accomplishments

We have accomplished the following tasks:

- The dose accuracy for MR-based treatment planning of prostate cancer has been validated using the Monte Carlo method and demonstrated consistent results.
- A practical method for heterogeneity correction for MRI-based dose calculation in inhomogeneous patient anatomy has been developed.
- A practical technique to create MR-based DRRs for prostate IMRT has been developed that can be used for patient setup when MR-based treatment planning is applied clinically.

Reportable Outcomes

Peer-reviewed papers resulting from or supported in part by this grant:

- **Chen L**, Nguyen T-B, Jones E, Chen Z, Luo W, Wang L, Price RA, Pollack A and Ma C-M. MRI-Based Treatment Planning for Prostate IMRT: Creation of Digitally Reconstructed Radiographs (DRR). *International Journal of Radiation Oncology Biology Physics* (2007a) accepted
- Chen Z, Ma C-M, Paskalev K, Li J, Yang J, Richardson T, Palacio L, Xu X and **Chen L**. Investigation of MR Image Distortion for Radiotherapy Treatment Planning of Prostate Cancer. *Phys. Med. Biol.* 51: 1393-1404 2006
- Chen Z, Ma C-M, Yang J, Li J, Luo W, Fan J, Paskalev K.A, Price Jr R A, Chen Y and **Chen L**. Monte Carlo dose verification of MR image based IMRT treatment planning for prostate cancer. *The XVth International Conference on the use of Computers in Radiation Therapy*, submitted 2007b
- Fan, J., Li, L., **Chen, L.**, Stathakis, S., Luo, W., du Plessis, F., Xiong, W., Ma, C.-M. A Practical Monte Carlo MU Verification Tool for IMRT Quality Assurance. *Phys. Med. Biol.* 51: 2503-15, 2006.
- Luo, W., Li, J.S., Price, R.A., **Chen, L.**, Yang, J., Fan, J., Chen, Z., McNeeley, S., and Ma, C.-M. Monte Carlo based IMRT QA using MLC log files and R/V outputs, *Med. Phys.* 33: 2557-64, 2006.

- Wang, L., Li, J., Paskalev, K., Hoban, P., Luo, W., **Chen, L.**, McNeeley, S., Price, R., Ma, C.-M. Commissioning and quality assurance of a commercial stereotactic treatment planning system for extracranial IMRT. *JACMP*, 7: 21-34, 2006.
- Wang, L., Feigenberg, S., **Chen, L.**, Paskalev, K., Ma, C.-M. Benefit of 3D image-guided stereotactic localization in the hypofractionated treatment of lung cancer. *Int. J. Rad. Oncol. Bio. Phys.* 66: 738-747, 2006.

Chapters:

- Y Cao and **Chen L.** Current MRI Application in Radiation Oncology. AAPM Summer School 2006

Meeting abstracts resulting from or supported in part by this grant:

- **Chen L.**, Xu X, Wang L, Paskalev K, Price R, Feigenberg S, Horwit E, Pollack A, Ma C. Rectal Dose Variation in Image Guided Radiation Therapy of Prostate Cancer. *Medical Physics*, 33(6), 2189, 2006
- Chen Z, Ma C, Li J, Paskalev K, Price R, Luo W, Fan J, Stathakis S, Che Y, Lin T, **Chen L.** Effect of Voxel Size on Monte Carlo Dose Calculation for Intensity Modulated Radiotherapy Treatment Planning. *Medical Physics*, 33(6), 2095, 2006.
- Chen Z, Ma C, Li J, Paskalev K, Price P, Luo W, Fan J, Chen Y, T Lin T, **Chen L.** Monte Carlo Investigation of Dose Perturbation by Hip Replacements in Intensity Modulated Radiotherapy of Prostate Cancer. *Medical Physics*, 33(6), 2123, 2006.
- Fan J, Li J, **Chen L.**, Price R, Paskalev K, Chen Z, Stathakis S, Luo W, Ma C. Generic Source Models for Commonly Used Clinical Accelerator beams for Monte Carlo Treatment Planning. *Medical Physics*, 33(6), 2292, 2006
- Luo W, Li J, Price R, **Chen L.**, Fan J, Chen Z, Lin T, Wang L, C Ma. Developing a comprehensive patient-specific QA procedure for IMRT. *Medical Physics*, 33(6), 2247, 2006
- Ma C, Li J, Stathakis S, Leal A, DuPlessis F, Fan J, Chen Y, **Chen L.**, McNeeley S, Price R. Advanced Mixed Beam Radiotherapy for Breast and Head and Neck. *Medical Physics*, 33(6), 2256, 2006
- Wang L, Feigenberg S, Paskalev K, **Chen L.**, Ma C. Benefit of 3D image-guided stereotactic localization in the hypofractionated treatment of lung cancer. *Proc. Medical Physics*, 33(6), 1993, 2006.
- Wang L, Feigenberg S, **Chen L.**, Paskalev K, Jin L, Ma C. How to account for patient-specific tumor motion in target definition for lung cancer treatment planning: Dosimetric comparison of a multi-phase CT simulation approach and MRI cine study. *Proc. Medical Physics*, 33(6), 2037, 2006.

- Wang L, Feigenberg S, **Chen L**, Paskalev K, Jin L and. Ma C.C.M. On Accounting for Patient-Specific Tumor Motion in Target Definition for Lung Cancer Treatment Planning: Comparison of a Multi-Phase CT Simulation Approach and MRI CINE Study. *International Journal of Radiation Oncology*Biology*Physics*, Volume 66, Issue 3, Supplement 1, 1 November S612-S613. 2006.

Funding applied for based on work resulting from or supported in part by this grant:

None

Conclusions

We have made significant progress during our third year investigation. We have successfully performed the tasks scheduled in the “Statement of Work”. We have developed a practical technique to create MR-based DRRs for prostate IMRT that can be used for patient setup when MR-based treatment planning is applied clinically. We have developed guidelines for MRI-based treatment planning dose calculation and quality assurance programs for MRI simulation for prostate cancer treatment.

Note on Human Subject Protection Approval

We have an approved IRB (IRB# 04-848) by both Fox Chase Cancer Center and DOD for this project.

References

Chen L, Nguyen T-B, Jones E, Chen Z, Luo W, Wang L, Price RA, Pollack A and Ma C-M. MRI-Based Treatment Planning for Prostate IMRT: Creation of Digitally Reconstructed Radiographs (DRR). *International Journal of Radiation Oncology Biology Physics* (2007a) accepted

Chen Z, Ma C-M, Paskalev K, Li J, Yang J, Richardson T, Palacio L, Xu X and **Chen L**. Investigation of MR Image Distortion for Radiotherapy Treatment Planning of Prostate Cancer. *Phys. Med. Biol.* 51: 1393-1404 2006

Chen Z, Ma C-M, Yang J, Li J, Luo W, Fan J, Paskalev K.A, Price Jr R A, Chen Y and **Chen L**. Monte Carlo dose verification of MR image based IMRT treatment planning for prostate cancer. *The XVth Internatinal Conference on the use of Computers in Radiation Therapy*, submitted 2007b

Chen L, Price RA Jr., Wang L, Li JS, Qin L, Ding M, Palacio E, T-B Nguyen, Ma C-M, Pollack A. Dosimetric evaluation of MRI-based treatment planning for prostate cancer. *Phys. Med. Biol.* 49: 5157-5170 (2004a).

Chen L, Price RA Jr., Wang L, Li JS, Qin L, Shawn M, Ma C-M, Freedman GM and Pollack A . MRI-Based Treatment Planning for Radiotherapy: Dosimetric Verification for Prostate IMRT. *International Journal of Radiation Oncology Biology Physics* 60(2): 636-47 (2004b)

Ma C-M, Mok E, Kapur A, Findley D, Brain S, Forster K and Boyer A L. Clinical implementation of a Monte Carlo treatment planning system, *Med. Phys.* 26:2133-43 (1999)

Ma C M, Pawlicki T, Jiang S B, Mok E, Kapur a., L. Xing, L. Ma and A.L. Boyer, Monte Carlo verification of IMRT dose distributions from a commercial treatment planning optimization system, *Phys. Med. Biol.*, 45:2483-95 (2000)

Ma C-M, Li J S, Pawlicki T, Jiang S.B, Deng J, A Monte Carlo dose calculation tool for radiotherapy treatment planning, *Med. Phys.* 47:1671-89 (2002)

Appendices

List of manuscripts quoted in the body of text:

Chen L, Nguyen T-B, Jones E, Chen Z, Luo W, Wang L, Price RA, Pollack A and Ma C-M. MRI-Based Treatment Planning for Prostate IMRT: Creation of Digitally Reconstructed Radiographs (DRR). *International Journal of Radiation Oncology Biology Physics* (2007a) accepted

Chen Z, Ma C-M, Paskalev K, Li J, Yang J, Richardson T, Palacio L, Xu X and **Chen L**. Investigation of MR Image Distortion for Radiotherapy Treatment Planning of Prostate Cancer. *Phys. Med. Biol.* 51: 1393-1404 2006

Chen Z, Ma C-M, Yang J, Li J, Luo W, Fan J, Paskalev K.A, Price Jr R A, Chen Y and **Chen L**. Monte Carlo dose verification of MR image based IMRT treatment planning for prostate cancer. *The XVth Internatinal Conference on the use of Computers in Radiation Therapy*, submitted 2007b

Elsevier Editorial System(tm) for International Journal of Radiation Oncology*Biology*Physics

Manuscript Draft

Manuscript Number:

Title: MRI-Based Treatment Planning for Prostate IMRT: Creation of Digitally Reconstructed Radiographs (DRR)

Article Type: Full Length Article

Section/Category: Clinical Investigation

Keywords: Radiotherapy, MRI treatment planning, Prostate Cancer, MRI-based DRRs

Running Title: MRI-based DRRs for Prostate Cancer

Corresponding Author: Dr. Lili Chen, PhD

Corresponding Author's Institution: Fox Chase Cancer Center

First Author: Lili Chen, PhD

Order of Authors: Lili Chen, PhD; Thai-Binh Nguyen, M.S; Elan Jones; Zuoqun Chen, PhD

Manuscript Region of Origin:

Abstract: Purpose: Recent studies demonstrated that MRI-based treatment planning meets the dosimetric accuracy for prostate intensity-modulated radiation therapy (IMRT) and it is adequate to use unity density in treatment planning dose calculation for prostate after correction of MRI distortions. The purpose of this study is to develop a technique to create MR-based digitally reconstructed radiographs (DRR) for patient initial setup for routine clinical applications of MR-based treatment planning for prostate IMRT.

Materials and Methods: Twenty prostate patients' CT and MR images were used for the study. CT and MR images were fused. The pelvic bony structures including femoral heads, pubic rami, ischium and ischial tuberosity that are relevant for routine clinical patient setup were manually contoured on axial MR images using the AcQsim planning system. The contoured bony structures were then assigned a bulk density of 2.0

g/cm³. The MRI based DRRs were generated. The accuracy of the MR based DRRs was quantitatively evaluated by comparing MR-based DRRs with CT-based DRRs for these patients. For each patient 8 measuring points on both coronal and sagittal DRRs were used for quantitative evaluation.

Results: The maximum difference in the mean values of these measurement points is 1.3 ± 1.6 mm and the maximum difference in absolute positions is within 3 mm for the 20 patients investigated.

Conclusions: MR-based DRRs are comparable to CT-based DRRs for prostate IMRT and can be used for patient treatment setup when MR-based treatment planning is applied clinically.

**MRI-Based Treatment Planning for Prostate IMRT: Creation of Digitally
Reconstructed Radiographs (DRR)**

Lili Chen Ph.D., Thai-Binh Nguyen M.S., Elan Jones., Zuoqun Chen Ph.D., Wei Luo Ph.D.,
Lu Wang Ph.D., Robert A Price Jr. Ph.D., Elan Jones., Alan Pollack Ph.D., M.D.
and C-M Charlie Ma, Ph.D

Radiation Oncology Department
Fox Chase Cancer Center
Philadelphia, PA 19111, USA

Submitted to IJROBP

Please send correspondence to:

Lili Chen, Ph.D.

Radiation Oncology Department
Fox Chase Cancer Center
333 Cottman Av.
Philadelphia, PA 19111, USA
Tel.: (215) 728-3003
Fax: (215) 728-4789
Email: lili.chen@fccc.edu

The materials in this paper have been partially presented at the AAPM 2004
Annual Meeting in Pittsburgher

Running title: Creation of MR-based DRRs for prostate IMRT

Conflicts of Interest Notification

The actual or potential conflicts of interest : No

Abstract

Purpose: Recent studies demonstrated that MRI-based treatment planning meets the dosimetric accuracy for prostate intensity-modulated radiation therapy (IMRT) and it is adequate to use unity density in treatment planning dose calculation for prostate after correction of MRI distortions. The purpose of this study is to develop a technique to create MR-based digitally reconstructed radiographs (DRR) for patient initial setup for routine clinical applications of MR-based treatment planning for prostate IMRT.

Materials and Methods: Twenty prostate patients' CT and MR images were used for the study. CT and MR images were fused. The pelvic bony structures including femoral heads, pubic rami, ischium and ischial tuberosity that are relevant for routine clinical patient setup were manually contoured on axial MR images using the AcQsim planning system. The contoured bony structures were then assigned a bulk density of 2.0 g/cm^3 . The MRI based DRRs were generated. The accuracy of the MR based DRRs was quantitatively evaluated by comparing MR-based DRRs with CT-based DRRs for these patients. For each patient 8 measuring points on both coronal and sagittal DRRs were used for quantitative evaluation.

Results: The maximum difference in the mean values of these measurement points is $1.3 \pm 1.6 \text{ mm}$ and the maximum difference in absolute positions is within 3 mm for the 20 patients investigated.

Conclusions: MR-based DRRs are comparable to CT-based DRRs for prostate IMRT and can be used for patient treatment setup when MR-based treatment planning is applied clinically.

Keywords: Radiotherapy, MRI treatment planning, Prostate Cancer, MRI-based DRRs

Running Title: MRI-based DRRs for Prostate Cancer

Introduction

Magnetic resonance imaging (MRI) provides superior image quality for soft tissue delineation over computed tomography (CT) and is widely used for target and organ delineation in radiotherapy for treatment planning (1-4). The prostate CTV appears to be overestimated with CT images compared with MRI (3, 5). The prostate volume on CT appears to be approximately 40% larger than on MRI reported by Rasch (5). These results were consistent with those reported by Krempien et al (6). Sannazzari et al (3) also showed a mean overestimation of CTV of 34% with CT compared with MRI. Results showed that radiation doses received by the penile bulb and corporal bodies may cause erectile dysfunction after prostate treatment (7). Studies are being performed at Fox Chase Cancer Center (FCCC) to use MRI to limit the dose to the erectile tissue with intensity-modulated radiation therapy (IMRT). A Phase III randomized trial at FCCC has investigated the clinical significance of the erectile tissue-sparing technique. Recently, Steenbakkers et al (8) also reported that the dose delivered to the rectal wall and bulb of the penis was significantly reduced in treatment plans based on MRI-delineated prostates compared with CT-delineated prostates, allowing a dose escalation of 2.0-7.0 Gy for the same rectal wall dose.

Recent studies suggest that dose escalation with 3D conformal radiotherapy (3DCRT) or IMRT can potentially improve local control and toxicity (9-18). Currently, the gold standard for prostate treatment planning is to use both CT and MR imaging to take the advantage of the electron density information with the CT and the superior soft tissue capabilities with MRI. Ideally, treatment planning would be based solely on a clinically useful diagnostic MR study. The advantages of MR-based treatment planning are 1) to

remove potential errors due to image fusion; 2) to reduce patient cost by avoiding redundant CT scans; and 3) to eliminate unnecessary radiation exposure to the patient and to save patient, staff and machine time. However, there are several challenges to directly using MR images for treatment planning, including (1) the lack of electron density information that is needed for heterogeneity corrections in dose calculation, (2) image distortion that affects patient external contour determination and therefore introduces dose calculation uncertainty, and (3) lack of bony structures to derive effective DRRs for patient setup. The first two issues, i.e. the lack of electron density information and image distortions in MR-based prostate treatment planning have been discussed in great detail by Chen et al (19). The purpose of this study is to investigate a technique to create MR-based DRRs for prostate IMRT patient setup when MR-based treatment planning is applied clinically.

Material and Methods

Image collection

CT-MR fusion with CT-based dose calculation has been a routine procedure for prostate IMRT treatment planning at FCCC since 2001. CT-based DRRs together with BAT (B-mode Acquisition and Targeting, NOMOS, Corp., Sewickley, PA) ultrasound or the CT-on-rails system (Siemens Medical Solutions, Concord, CA) are used for initial patient setup and target localization. On-line images, obtained from either the CT-on-rails system or the BAT ultrasound system were used for daily target localization to correct for prostate inter-fraction motion. For this study, twenty patients with fused CT-MR images were used.

Calibration of bony structures on MRI

Figure 1 shows an example of the DRR directly created from MR images. It is clearly demonstrated that the DRRs do not provide enough bony structure information for patient positioning verification. Therefore, it is necessary to develop a technique for the creation of useful MR-based DRRs for initial treatment setup when CT is not involved. Clinical bony landmarks such as pubis, ischium and ischial tuberosity on CT-based DRRs are used to adjust the patient treatment position by comparing with anterior-posterior (AP) and lateral portal images. Our goal is to develop a technique to create MR-based DRRs that are comparable to CT-based DRRs for the clinical implementation of MR-based treatment planning for prostate IMRT. Our approach is to generate MR-based DRRs by contouring the relevant bony structures and assign them with a bulk density. We performed this study on an AcQsim system (Philips Medical System, Cleveland, OH).

On T2 weighted MR images, bones appear hyperintense (white) surrounded by narrow hypo-intense (dark) regions. The marrow inside the bone or soft bones shows high intensity (white) while compact bone shows lower intensity (dark). Therefore, the boundary between the bone and the soft tissue is not always distinguishable on MRI. In order to study the correlation between CT number (electron density) and MR signal intensity, CT and MR images were fused according to bony anatomy using the interactive method available on the AcQsim system. CT images were loaded as primary images and MR images were loaded as secondary images. The two images were shown side by side on the same computer screen. The bones were contoured based on CT images while the contours were also shown on MRI simultaneously. The calibration of the bones on MRI that are relevant

to prostate treatment setups was established based on CT images. Based on this calibration, the boundary of each relevant bone can be easily determined on MRI alone.

Guidelines for bone contouring

The technique that we describe here is intended to serve as a guide for the clinical implementation of MR-based treatment planning for prostate cancer. We outline contours of the bones at the level of the top of the femoral head (a) to the lesser trochanter of the femur (b) as shown in Figure 2. In order to describe our contour technique clearly we categorize the pelvic bones into three groups according to the similarity of the bone shape as shown in Figure 2. Figure 3 shows the correlation of the bony contours on the axial MR image and contour lines on the coronal and sagittal MR images. Critical points for each group are determined based on the relation of the points on the DRR that are used for checking patient positions routinely.

For convenience, we have defined a few technical terms for our contouring technique including “white side (strict)”, “white side (non-strict)”, “dark side (strict)”, and “dark side (non-strict)”. The term “white” indicates the hyper-intense region on the T2 weighted image and “dark” indicates the hypo-intense region on the T2 weighted image. Thus, “white side (strict)” means to draw a contour immediately outside the hyper-intense region and “white side (non-strict)” means the contour is drawn slightly away from the hyper-intense region (about 1 pixel away), as shown in Figures 4. The same concept can be applied to the terms “dark side (strict)” and “dark side (non-strict)”. As mentioned previously we divided the pelvic region into 3 groups. For each group the left and right

bones are mirror images on the axial view. Therefore we only describe our method for the right-side bones. To start contouring, “Virtual fluoroscopy” is selected on the tool menu, which displays the three dimensional views of the MR images. The contours are drawn on the axial images slice by slice while the contours will show simultaneously on both coronal and sagittal views.

Contouring bony structures for the first group (region 1)

The points of interest (POI) here are “A” and “B” (see Figure 5) that will determine points “a” and “b” on the coronal DRR and “a” on the sagittal DRR (see Figure 9). Point “C” was found not critical for patient setup that will appear as “b” on the sagittal DRR.

To contour POI A, one can imagine that there are 2 lines “a” and “b” on two sides of the peak. The intersection of “a” and “b” is the POI A. Lines “a” and “b” are determined based on the boundary between hyper- and hypo-intense regions using the “white side (non-strict)” technique. POI B is the intersection of the straight lines between black side and white side as shown in Figure 6. It should be mentioned that the exact locations of the POI points will affect the accuracy of the resulting DRR while the volumes of the contoured structures will not.

Contouring bony structures for the second group (region 2)

There are two relevant bones in region 2 including pubic symphysis and ischial tuberosity. As shown in Figure 7, POI A and POI C are critical for the positioning check clinically while POI B, E and D are not critical. For point A the vertical line is contoured with “white

side (strict)". Attention should be paid to the horizontal line here because its height will appear on the sagittal DRR that will be used to judge the patient AP position. The horizontal line is contoured with "white side (strict)". We draw the horizontal line starting from where the white (hyper-intense) begins to blur. For POI C we use the same method as for POI B of the first group. For POI B, E and D we contour with "white side (non-strict)" since they are not critical to patient setups.

Contouring bony structures for the third group (region 3)

For the third group, only POI A is the critical point. The way to determine this point is similar to that for POI A for the first group. This means that POI A is the intersection of two lines: one is on top (white side) and the other is the dark side (non-strict) of the gap as shown in Figure 8.

Creation of MR-based DRRs

After contouring the three bone groups, proper names were given to these bones in the "organ selection" menu (e.g., symphysis). A bulk electron density was assigned to these bones. Based on our experience an electron density between 1.8 and 2.0g/mm³ is adequate. After assigning electron densities to all the relevant bones the DRRs were generated. The quality of the coronal and lateral DRRs can be improved by adjusting the window and level parameters. Figure 9 shows the MR-based DRR and the CT-based DRR for one of the 20 patients investigated.

Data analysis

Paired MR-based and CT-based DRRs were compared quantitatively for all the patients investigated. Contoured bony structures from MRI were superimposed on CT-based DRRs using the Photoshop software with the same isocenter (Figure 10). The 8 points from both coronal and sagittal DRRs were used for the comparison. The difference for each position point between CT and MRI was calculated based on the pixel value. Minus values mean the position points on MR-based DRRs were inside the outlines of the corresponding bony structures on the CT-based DRRs while positive values mean the MR-determined position points were outside the outlines of bony structures on the CT-based DRRs. The mean and 1 standard deviation of the error for each measurement point were calculated for 20 patients. The maximum differences between CT and MR for each measurement point were also calculated.

Results and discussions

In this work, we have developed a method to generate MR-based DRRs for the clinical implementation of MRI-based treatment planning for prostate IMRT. Figure 9 shows MR-based DRRs and CT-based DRRs for one of the patients investigated in this work. The MR-based DRRs were generated with a 2.0 g/cm^3 density assigned to the relevant bony structures. It demonstrates that MR-based DRRs are comparable to CT-based DRRs and it is reasonable to use 2.0 g/cm^3 as the bulk density. In fact, one can also select to print MR-based DRRs with the outlined bony contours on top of the gray-scale image. This way, the contour lines (instead of the gray-scale image) on the DRRs can be directly used to compare the bony structures on a portal film or an EPID image (see Figure 10).

To evaluate the accuracy of the MR-based DRRs generated using our method, we have selected 8 relevant position points on coronal and sagittal DRRs to compare the actual locations of the relevant bony structures. The differences of the position points between MR-based DRRs and CT-based DRRs for 20 patients are summarized in Table 1. Since the patients' CT and MR images were directly taken from our clinical data base and they were already fused for treatment planning the positional differences shown here also included the positional errors due to the fusion process, which is estimated to be about 2mm. The agreement between MR-based DRRs and CT-based DRRs is excellent. The mean difference is within 0.8 ± 1.5 mm except for point 7 (1.3 ± 1.6) mm and the maximum difference is within 3.0 mm for all 180 position points evaluated for the 20 patients except for point 7 of patient 19 (3.6mm). From a clinical point of view, point 7 is less important than point 8 (pubis) that is used for the determination of the patient AP positions. These results demonstrate that there is no systematic biasing in our contouring method.

It should be noted that on the coronal DRR all the bones (and position points) have mirror images and therefore their relative positions are less affected by the contouring method used as long as they are contoured consistently. For example, if the symphysis is contoured consistently between the left side and the right side the midline of the symphysis (i.e., the left-right position of the patient) determined by points 3 and 4 will be accurate even though the absolute positions of points 3 and 4 may be affected by the contouring method or by inter-personal variations. The same can be said about the patient superior-inferior position which can be accurately determined by bony landmarks such as pubis and ischium through paired points such as (1, 5) and (2, 6). The patient AP position is mainly determined based

on the pubis position (i.e., point 8 on the sagittal DRR). Again, the relative position determined by a bony structure is expected to be more accurate than the absolute positions of the contour points defining the bony structure. The same phenomenon can be observed with gray-scale images when different “window” and “level” parameters are used. Based on this analysis we estimate the accuracy of our MR-based DRRs is about 3 mm or better. This does not include the uncertainties introduced by the CT-MRI fusion process since they will be eliminated when MRI alone is used for radiotherapy treatment planning.

MR-based DRRs can be used for initial patient position verification by comparing with images taken using portal film or an EPID. In our clinical implementation of MRI-based treatment planning for prostate IMRT, MRI-based DRRs are used during initial treatment setups together with either a BAT or a CT-on-rails system to set the baseline treatment position. The 3 mm accuracy for MR-based DRRs is considered adequate for this purpose. In fact, for routine prostate IMRT treatment at FCCC, we use the BAT ultrasound system or the CT-on-rails system as a primary means to relocate the soft tissue target prior to each treatment. The initial patient setup based on portal film or EPID only serves as a secondary means to place the treatment target 0.5 – 0.7 cm within the treatment isocenter. This will facilitate the target localization process in the subsequent daily treatments. Table 2 shows the mean shift values of the 38 treatment fractions for the first 4 prostate IMRT patients planned using MRI alone and 4 other prostate IMRT patients planned using CT alone, being treated at the same time. The shift values in the three major axes were all within expected values. Occasionally larger shifts (>1cm) were observed for both CT- and MRI-based planning when large gas pockets occurred in the rectum. The combined target

localization accuracy for routine prostate treatment is expected to be better than 5 mm at 95% confidence level.

Finally, we also investigated the time required to generate MR-based DRRs. Although manual contouring is needed for making practical MR-based DRRs the time required to contour all relevant bones for a patient was approximately 10-15 minutes. The time to assign a bulk electron density to the relevant bony structures was minimal. In fact, it is not necessary to contour the femoral head since the pubis (symphysis), ischium and ischial tuberosity positions are sufficient to determine the patient positions. We have contoured femoral heads to provide redundant checks and more realistic DRRs.

In summary, we have explored the use of MR-based DRRs for initial radiotherapy treatment setup verification for prostate IMRT by comparing with images taken using portal film or EPID. Our results showed that MR-based DRRs utilizing the outlines of relevant bony structures have an accuracy of about 3 mm, which are adequate for initial patient setup. This technique has been used, in combination with the BAT/in-room CT daily target localization technique, for the clinical implementation of MRI-based treatment planning for prostate IMRT at FCCC since Nov. 2003.

Acknowledgments

This project was supported in part by grants from the DOD (PC030800), the NIH (CA78331) and the Howard Hughes Medical Institute. We would also like to thank David

Abraham for his excellent technical assistance. We are indebted to Dr Gerald E Hank for his foresight in initiating MRI-simulation at Fox Chase Cancer Center.

References

1. Khoo VS, Adams EJ, Saran F, *et al.* A Comparison of clinical target volumes determined by CT and MRI for the radiotherapy planning of base of skull meningiomas. *Int J Radiat Oncol Biol Phys* 2000; 46:1309-1317.
2. Potter R, Heil B, Schneider L, *et al.* Sagittal and coronal planes from MRI for treatment planning in tumors of brain, head and neck: MRI assisted simulation. *Radiother Oncol* 1992;23:127-130.
3. Sannazzari GL, Ragona R, Ruo Redda MG, *et al.* CT-MRI image fusion for delineation of volumes in three-dimensional conformal radiation therapy in the treatment of localized prostate cancer. *Br J Radiol* 2002;75:603-607.
4. Tanner. Radiotherapy planning of the pelvis using distortion corrected MR images: the removal of system distortions *Phys Med Biol* 2000;45:2117-2132.
5. Rasch C, Barillot I, Remeijer P, *et al.* Definition of the prostate in CT and MRI: a multi-observer study. *Int J Radiat Oncol Biol Phys* 1999;43:57-66.
6. Krempien RC, Schubert K, Zierhut D, *et al.* Open low-field magnetic resonance imaging in radiation therapy treatment planning. *Int J Radiat Oncol Biol Phys* 2002;53:1350-1360.

7. Buyyounouski MK, Horwitz EM, Uzzo RG, *et al.* The radiation doses to erectile tissues defined with magnetic resonance imaging after intensity-modulated radiation therapy or iodine-125 brachytherapy. *Int J Radiat Oncol Biol Phys* 2004;59:1383-1391.
8. Steenbakkers RJ, Deurloo KE, Nowak PJ, *et al.* Reduction of dose delivered to the rectum and bulb of the penis using MRI delineation for radiotherapy of the prostate. *Int J Radiat Oncol Biol Phys.* 2003;57:1269-1279.
9. Amer AM, Mott J, Mackay RI, *et al.* Prediction of the benefits from dose-escalated hypofractionated intensity-modulated radiotherapy for prostate cancer. *Int J Radiat Oncol Biol Phys* 2003;56:199-207.
10. Hanks GE. Progress in 3D conformal radiation treatment of prostate cancer. *Acta Oncol* 1999;38 Suppl 13:69-74.
11. Hanks GE, Hanlon AL, Schultheiss TE, *et al.* Dose escalation with 3D conformal treatment: five year outcomes, treatment optimization, and future directions. *Int J Radiat Oncol Biol Phys* 1998;41:501-510.
12. Hunt MA, Zelefsky MJ, Wolden S, *et al.* Treatment planning and delivery of intensity-modulated radiation therapy for primary nasopharynx cancer. *Int J Radiat Oncol Biol Phys* 2001;49:623-632.

13. Pollack A. Preliminary results of a randomized radiotherapy dose-escalation study comparing 70 Gy with 78 Gy for prostate cancer. *Journal of clinical oncology* 2000;23:3304-3911.
14. Pollack A, Zagars GK, Rosen, II. Prostate cancer treatment with radiotherapy: maturing methods that minimize morbidity. *Semin Oncol* 1999;26:150-161.
15. Pollack A, Zagars GK, Starkschall G, *et al.* Prostate cancer radiation dose response: results of the M. D. Anderson phase III randomized trial. *Int J Radiat Oncol Biol Phys* 2002;53:1097-1105.
16. Wachter S, Wachter-Gerstner N, Bock T, *et al.* Interobserver comparison of CT and MRI-based prostate apex definition. Clinical relevance for conformal radiotherapy treatment planning. *Strahlenther Onkol* 2002;178:263-268.
17. Yeoh EE, Fraser RJ, McGowan RE, *et al.* Evidence for efficacy without increased toxicity of hypofractionated radiotherapy for prostate carcinoma: early results of a Phase III randomized trial. *Int J Radiat Oncol Biol Phys* 2003;55:943-955.
18. Zelefsky MJ, Leibel SA, Gaudin PB, *et al.* Dose escalation with three-dimensional conformal radiation therapy affects the outcome in prostate cancer. *Int J Radiat Oncol Biol Phys* 1998;41:491-500.

19. Chen L, Price RA, Jr., Wang L, *et al.* MRI-based treatment planning for radiotherapy: dosimetric verification for prostate IMRT. *Int J Radiat Oncol Biol Phys* 2004;60:636-647.

Figure Legends

Figure 1. Digitally reconstructed radiographs (DRR) from MRI (a) and CT (b). Top figures are coronal view and bottom figures are sagittal view of the pelvic region.

Figure 2. Delineation of bony structures for MR-based DRRs showing contours starting at the level of the femoral head (a) to the lesser trochanter of the femur (b). The pelvic bones are divided into three groups according to the similarity of the bone shapes.

Figure 3. Correlations of the relevant bone contours on axial and coronal views (a) and axial and sagittal views (b). Detailed descriptions are given in the text.

Figure 4. Demonstration of the contouring technique: (a) “Contour White side (strict)” means contouring immediately outside the hyper-intense region, (b) “Contour white side (non-strict)” means contouring slightly away from the hyper-intense region (by about 1 pixel).

Figure 5. An example of the first bone group. POI A is correlated to both the coronal and sagittal DRRs while POI B is correlated to the coronal DRR and POI C is correlated to the sagittal DRR only.

Figure 6. An example to delineate POI A and POI B: they are the intersection points of the lines “a” and “b” (a); The volume defined by the contours away from the POIs will not affect the accuracy of the DRR (b).

Figure 7. An example of the second bone group and the correlation of the axial contours with the coronal and sagittal DRRs.

Figure 8. An example of the third bone group and the correlation of the axial contours with the coronal and sagittal DRRs.

Figure 9. An example of MR-based DRRs (a) and CT-based DRRs (b). The MR-based DRRs were generated after the relevant bones have been contoured and assigned to a bulk density of 2.0 g/cm^3 .

Figure 10. Measurement positions on coronal and sagittal DRRs to evaluate the accuracy of MR-based DRRs (characterized by the MR-based outlines/contour lines). Points 3 and 4 are used for the L-R position setup, points 1 and 5 or 2 and 6 are used for the I-S position setup, and points 7 and 8 are used for the A-P position setup.



Lili Chen Ph.D
Fox Chase Cancer Center
333 Cottman Av.
Philadelphia, PA 19111
Tel: 215 728 3003
Fax 215 728 4789
L_Chen@fccc.edu

James D. Cox, MD
Editor-in-Chief
International Journal of Radiation Oncology Biology Physics
Department Scientific Publications-227
1515 Holcombe Blvd.
Houston, TX 77030

Aug 14, 2006

Dear Dr. Cox:

We would like to submit our manuscript entitled "MRI-Based Treatment Planning for Prostate IMRT: Creation of Digitally Reconstructed Radiographs (DRR)" for publication in *International Journal of Radiation Oncology Biology Physics*.

The materials in this paper have been partially presented at the AAPM annual meeting in Pittsburgher 2004.

Yours sincerely,

A handwritten signature in cursive script that reads 'Lili Chen'.

Lili Chen, Ph.D.

Table 1 Distance (in mm) of measured position points between MR-based DRRs and CT-based DRRs.

Patient	Points of Measurement							
	1	2	3	4	5	6	7	8
1	1.3	-0.9	-1.7	-1.3	-1.7	-1.0	-2.2	-2.2
2	-1.0	-1.3	0.4	-2.2	-1.7	-2.0	0.9	0.4
3	0.0	-0.9	0.4	-1.3	-0.4	0.4	-1.3	-1.3
4	0.4	0.4	-2.2	0.9	-0.9	-1.0	0.9	-1.7
5	0.4	0.4	0.9	-1.3	-0.9	2.2	0.4	-0.9
6	1.3	0.9	-1.7	-0.9	-2.6	-3.0	0.9	0.9
7	0.9	-1.3	1.3	-1.7	0.4	0.4	3.0	3.0
8	0.4	0.4	-0.9	0.4	-1.3	0.9	1.3	1.3
9	0.4	-0.9	0.4	-0.4	-1.7	-2.0	0.4	1.7
10	2.2	-0.9	2.2	-1.3	-2.2	-1.0	1.3	0.0
11	1.3	2.2	1.7	-1.3	0.9	0.9	2.6	0.0
12	0.4	0.9	0.9	-1.3	-2.2	-2.2	2.2	1.7
13	0.9	-0.9	-0.9	-1.3	1.7	-1.3	0.9	-1.3
14	0.4	0.4	-2.2	0.9	-1.3	2.2	3.0	0.4
15	-2.0	1.7	1.7	1.3	2.2	1.7	2.2	-1.7
16	0.4	1.6	2.0	-0.8	2.0	2.8	2.4	1.2
17	-1.2	-1.6	-2.0	1.6	-1.6	-1.6	2.8	-2.0
18	-2.0	-1.6	-0.8	-1.6	-2.4	-1.6	-1.2	-2.8
19	-1.6	-2.4	-1.2	-2.4	-1.2	-0.8	3.6	2.0
20	-1.2	-0.8	1.2	1.2	-1.6	-0.4	1.6	0.8
mean ± SD	0.1±1.2	-0.2±1.3	-0.0±1.5	-0.6±1.2	-0.8±1.5	-0.3±1.6	1.3±1.6	-0.0±1.6
Max. diff	2.2	2.4	2.2	2.4	2.6	3.0	3.0	3.0

Table 2 Mean shift values along the three major axes based on the BAT ultrasound target localization procedures for 38 IMRT treatments. The shift values were calculated as the differences between the planned target locations and the actual target locations measured by the BAT system prior to each treatment. The initial treatment setups were using either CT-based DRRs or MR-based DRRs.

Patient #	Shifts based on MR-simulation (cm)		
	RL	AP	SI
1	-0.19 ± 0.25	0.07 ± 0.39	0.51 ± 0.43
2	-0.20 ± 0.32	0.31 ± 0.53	0.10 ± 0.48
3	0.15 ± 0.25	0.39 ± 0.23	0.78 ± 0.23
4	0.12 ± 0.29	0.53 ± 0.29	0.14 ± 0.29
Patient #	Shifts based on CT-simulation (cm)		
	RL	AP	SI
1	0.09 ± 0.42	-0.33 ± 0.30	-0.03 ± 0.34
2	0.28 ± 0.25	0.03 ± 0.42	0.48 ± 0.41
3	-0.01 ± 0.25	-0.06 ± 0.27	0.32 ± 0.32
4	0.05 ± 0.24	0.04 ± 0.17	0.40 ± 0.40

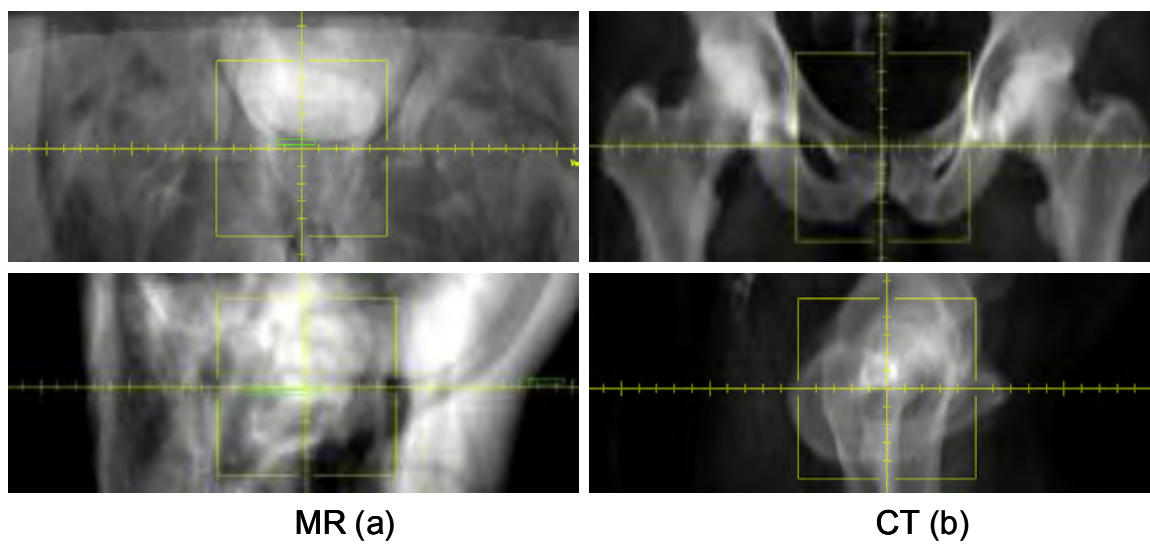


Figure 1. Digitally reconstructed radiographs (DRR) from MRI (a) and CT (b). Top figures are coronal view and bottom figures are sagittal view of the pelvic region.

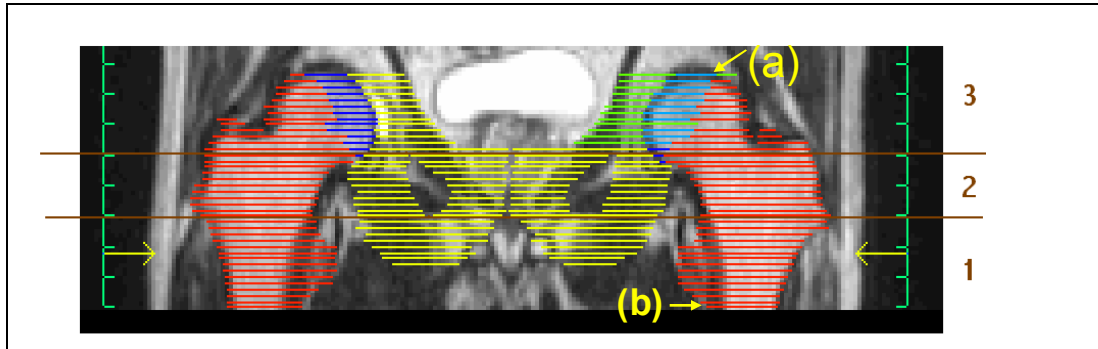
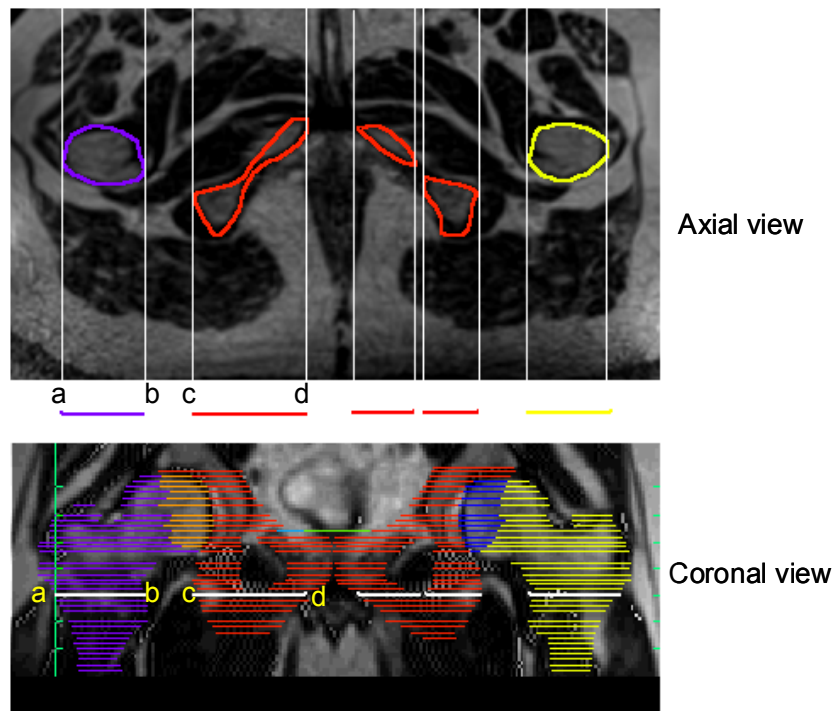
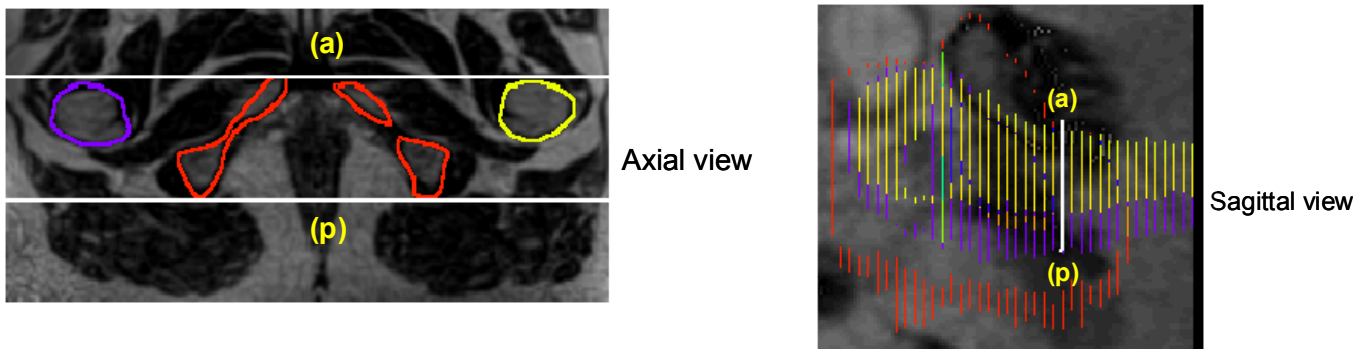


Figure 2. Delineation of bony structures for MR-based DRRs showing contours starting at the level of the femoral head (a) to the lesser trochanter of the femur (b). The pelvic bones are divided into three groups according to the similarity of the bone shapes.



(a)



(b)

Figure 3. Correlations of the relevant bone contours on axial and coronal views (a) and axial and sagittal views (b). Detailed descriptions are given in the text.



(a)



(b)

Figure 4. Demonstration of the contouring technique: (a) “Contour White side (strict)” means contouring immediately outside the hyper-intense region, (b) “Contour white side (non-strict)” means contouring slightly away from the hyper-intense region (by about 1 pixel).

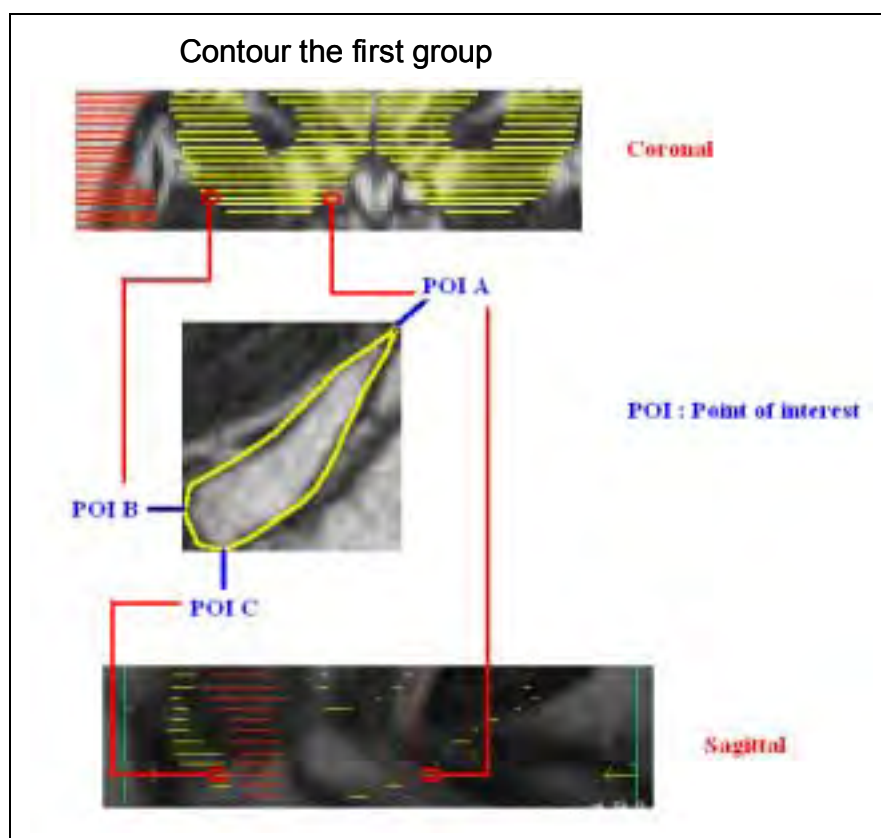


Figure 5. An example of the first bone group. POI A is correlated to both the coronal and sagittal DRRs while POI B is correlated to the coronal DRR and POI C is correlated to the sagittal DRR only.

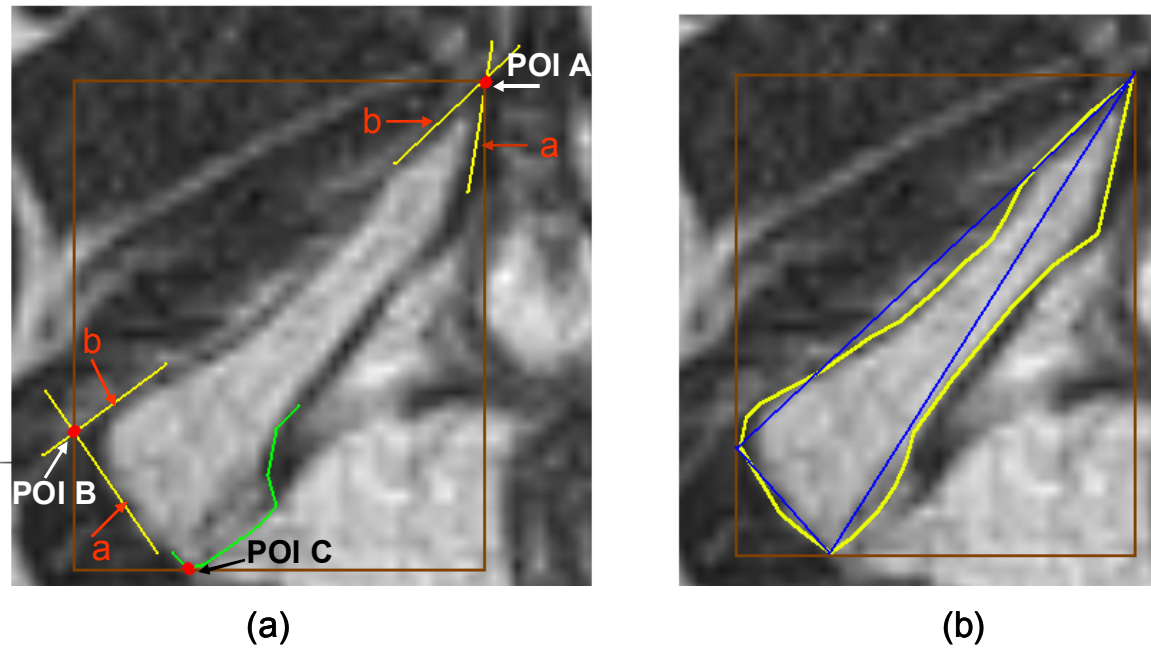


Figure 6. An example to delineate POI A and POI B: they are the intersection points of the lines “a” and “b” (a); The volume defined by the contours away from the POIs will not affect the accuracy of the DRR (b).

Figure 5. An example of the first bone group. POI A is correlated to both the coronal and sagittal DRRs while POI B is correlated to the coronal DRR and POI C is correlated to the sagittal DRR only.

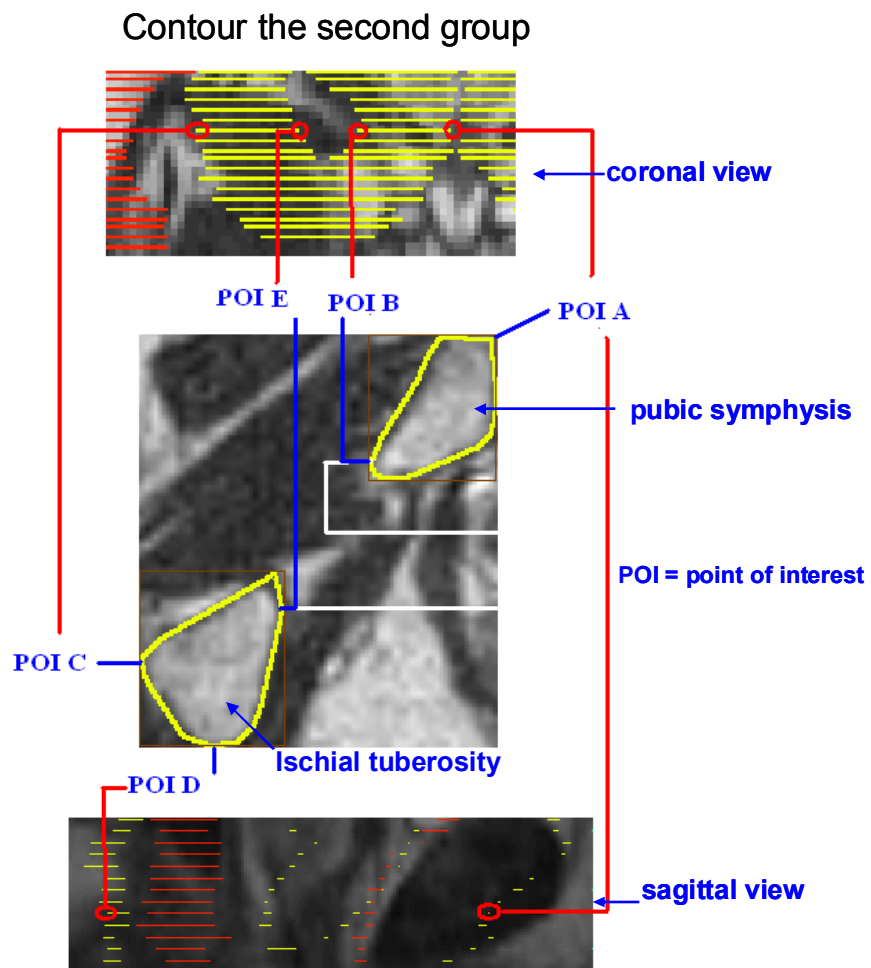


Figure 7. An example of the second bone group and the correlation of the axial contours with the coronal and sagittal DRRs.

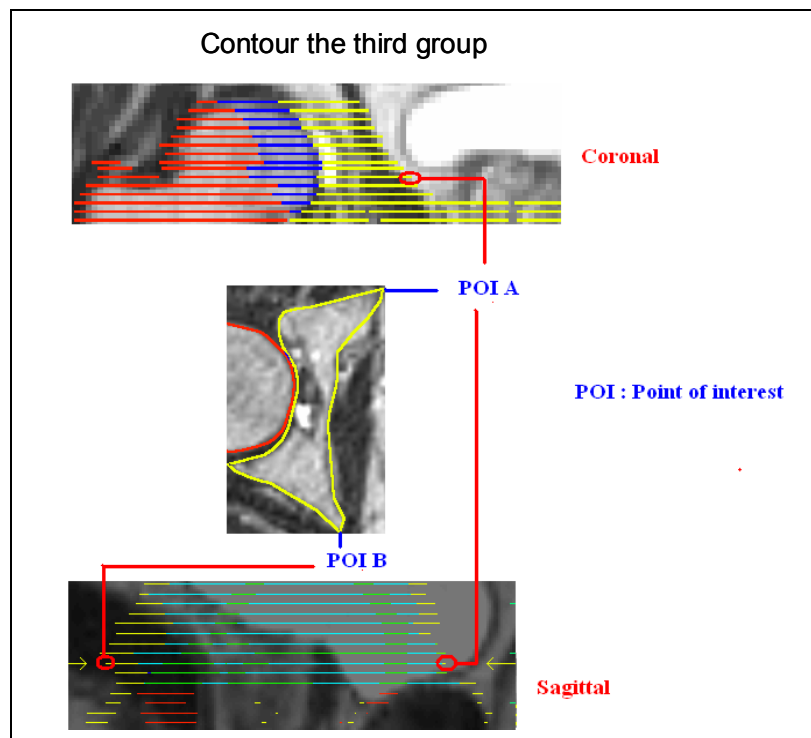


Figure 8. An example of the third bone group and the correlation of the axial contours with the coronal and sagittal DRRs.

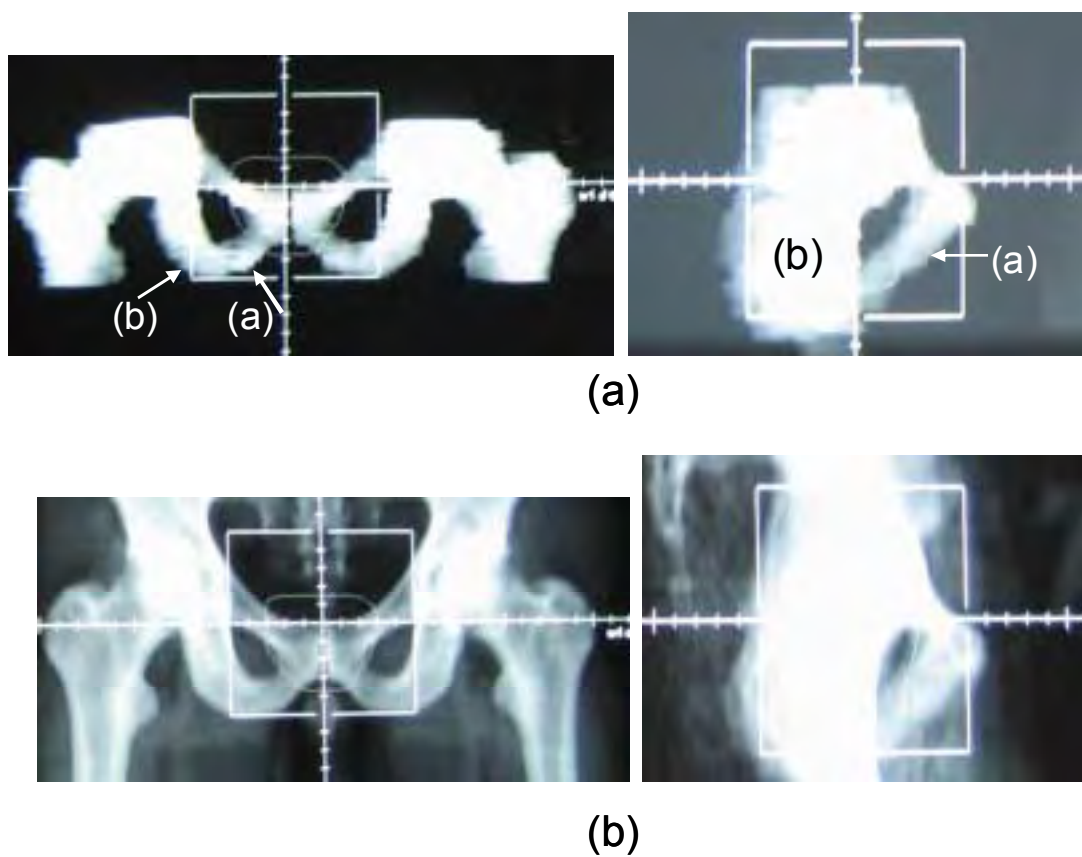


Figure 9. An example of MR-based DRRs (a) and CT-based DRRs (b). The MR-based DRRs were generated after the relevant bones have been contoured and assigned to a bulk density of 2.0 g/cm^3 .

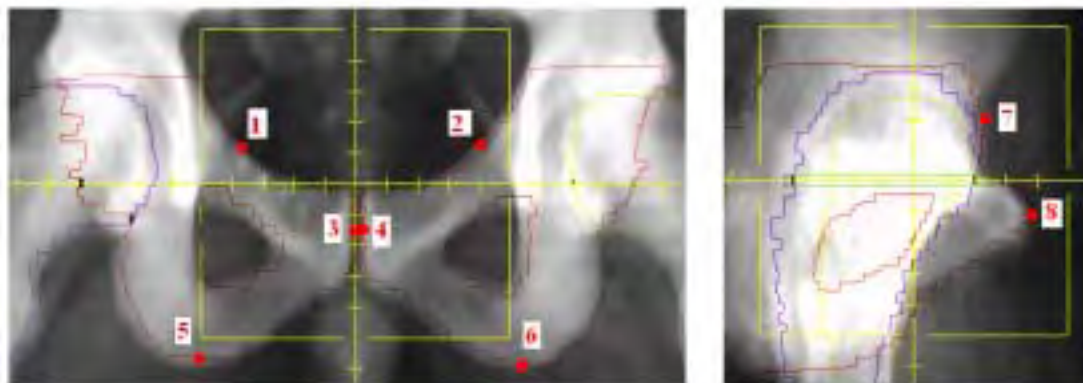


Figure 10. Measurement positions on coronal and sagittal DRRs to evaluate the accuracy of MR-based DRRs (characterized by the MR-based outlines/contour lines). Points 3 and 4 are used for the L-R position setup, points 1 and 5 or 2 and 6 are used for the I-S position setup, and points 7 and 8 are used for the A-P position setup.

Investigation of MR image distortion for radiotherapy treatment planning of prostate cancer

Z Chen, C-M Ma, K Paskalev, J Li, J Yang, T Richardson, L Palacio, X Xu and L Chen

Department of Radiation Oncology, Fox Chase Cancer Center, Philadelphia, PA 19111, USA

E-mail: jay.chen@fcc.edu

Received 12 September 2005, in final form 23 December 2005

Published 21 February 2006

Online at stacks.iop.org/PMB/51/1393

Abstract

MR imaging based treatment planning for radiotherapy of prostate cancer is limited due to MR imaging system related geometrical distortions, especially for patients with large body sizes. On our 0.23 T open scanner equipped with the gradient distortion correction (GDC) software, the residual image distortions after the GDC were <5 mm within the central 36 cm × 36 cm area for a standard 48 cm field of view (FOV). In order to use MR imaging alone for treatment planning the effect of residual MR distortions on external patient contour determination, especially for the peripheral regions outside the 36 cm × 36 cm area, must be investigated and corrected. In this work, we performed phantom measurements to quantify MR system related residual geometric distortions after the GDC and the effective FOV. Our results show that for patients with larger lateral dimensions (>36 cm), the differences in patient external contours between distortion-free CT images and GDC-corrected MR images were 1–2 cm because of the combination of greater gradient distortion and loss of field homogeneity away from the isocentre and the uncertainties in patient setup during CT and MRI scans. The measured distortion maps were used to perform point-by-point corrections for patients with large dimensions inside the effective FOV. Using the point-by-point method, the geometrical distortion after the GDC were reduced to <3 mm for external contour determination and the effective FOV was expanded from 36 cm to 42 cm.

(Some figures in this article are in colour only in the electronic version)

1. Introduction

Computed tomography (CT) has played a very important role in radiation treatment planning in modern radiotherapy. Based on the information provided by CT data, a treatment planning system can delineate patients' tumour volumes, external contours and critical anatomic

structures, obtain digitally constructed radiographs (DDR) for patient treatment set-up and perform accurate dose calculations for treatment planning. Although CT-based treatment planning has been considered as a 'gold standard' in radiotherapy for years, it has long been recognized as having poor soft tissue contrast, which may bring uncertainties into treatment planning. For example, Khoo *et al* (1999) found that MRI provided improved definitions of both prostate and critical structures compared to CT. Additionally, Rasch *et al* (1999) found that the prostate volume was 40% larger on CT than MR, in agreement with Roach *et al* (1996), who found that the prostate was 32% larger on CT than on MRI. Debois *et al* (1999) showed that improved rectal and prostate volume delineation from MRI could lead to improvement in both target coverage and rectal sparing. As many investigators have demonstrated (Zelevsky *et al* 1998, Pollack *et al* 1999, Pollack *et al* 2000, Hanks *et al* 1998, Hanks 1999), dose escalation with three-dimensional (3D) conformal and recently IMRT increases local control while reducing complications in nearby critical structures. However, as dose levels are increased, the precise knowledge of tumour volumes and the accuracy of dose calculation and delivery become critical. Magnetic resonance (MR) imaging has been shown to provide more consistent tumour volume delineation in treatment planning due to its superior soft tissue contrast than CT for a variety of sites.

Although CT and MR fusion has been widely accepted as a practical approach for both accurate delineation (using MR data) and dose calculation (using CT data) it would be ideal if MRI could replace CT entirely for treatment planning, retaining the superior soft tissue contrast for image segmentation and at the same time eliminating the potential errors in image fusion due to (a) variations in patient set-ups between CT and MR and (b) uncertainties in target localization between the two image modalities. Furthermore, MRI-based treatment planning will avoid redundant CT imaging sessions, which in turn will avoid unnecessary radiation exposure to patients, reduce treatment costs, and save patient, staff and machine time. There has been a growing interest in the utilization of MRI-based radiotherapy treatment planning for the past decade, and progress has been made in developing an effective MRI-based method for treatment planning (Beavis *et al* 1998, Guo 1998, Mah *et al* 2002, Chen *et al* 2002, Michiels *et al* 1994, Chen *et al* 2003, Lee and Bollet 2003).

It is well known that there are several technical challenges for MRI-based treatment planning: (1) to minimize MR image geometrical distortions, (2) to incorporate sequences that reduce MR distortions, (3) to develop methods that can correct MR-related distortions, (4) to correlate MR signal intensity with the densities of the materials imaged and (5) to obtain MRI-derived DRR for patient set-up.

We have been working extensively on developing MRI-based treatment planning models for the last few years (Chen *et al* 2003, 2004a, 2004b, 2004c). It has been generally accepted that there are no clinically significant differences in dose calculation between homogeneous and heterogeneous geometry for pelvis and it has been common practice to use homogenous geometry. We have implemented MRI-based prostate treatment planning at Fox Chase Cancer Center (FCCC). We have verified the dose calculation accuracy with unit-density geometry built for MR data. The agreement was within 2% with CT-based dose calculation (Chen *et al* 2004a). An effective procedure has been achieved to derive MRI-based DRRs for prostate cancer patient treatment set-up (Chen *et al* 2004b).

Our clinical MR unit (0.23 T open MR system, Philips Medical Systems, Cleveland, OH) is equipped with the gradient distortion correction (GDC) software (Mah *et al* 2002). Comparisons of patients' MR and distortion-free CT images showed that the systematic geometrical distortions were very small after the GDC for patients with 36 cm lateral dimensions and the dosimetric consequences due to these distortions were negligible for treatment planning. However, for patients with larger lateral dimensions, the differences in

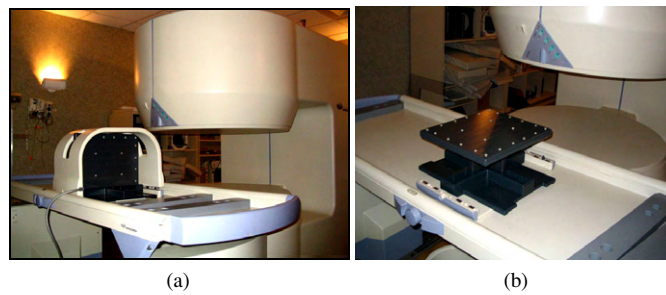


Figure 1. The Philips 0.23 Tesla open MR unit (a) and the F18 phantom (b). The F18 phantom with the support structure is placed in the body/spine coil. The support structure allows the marker plane to align with any selected imaging planes.

patient external contours between distortion-free CT images and GDC-corrected MR images were significant (1–2 cm) because of the combination of greater gradient distortion and loss of field homogeneity away from the isocentre and the uncertainties in patient set-up during CT and MRI scans. The uncertainties on the external contours will lead to errors in beam path length determination, which in turn may result in dose errors of clinical significance. In order to implement MR-based treatment planning clinically, the effective FOV of our MR scanner must be investigated and expanded to include patients with larger lateral dimensions.

In this paper, we present the results of our MR image distortion investigation on a 0.23 T open scanner for prostate IMRT treatment planning. A point-by-point mapping technique is developed to further reduce residual gradient distortions after GDC post-processing. We will describe the technical aspects of our method and its implementation and validation. We will show that together with set-up uncertainty quantification, the effective FOV of the scanner can be expanded to include almost all the prostate patients, and the uncertainties of patient external contours due to MR image distortions can be determined accurately.

2. Materials and method

2.1. The MR scanner

The MR system used for this study was a 0.23 Tesla open scanner operating clinically in the department of Radiation Oncology at Fox Chase Cancer Center (figure 1). The MR scanner consists of two approximately 1 m diameter poles. The separation between the two poles is 47 cm. The MR scan table can be moved in orthogonal planes along a set of rails mounted on the floor and on an orthogonal set of rails built in the couch. A flat table-top made of special material, which is stiff and light, was inserted beneath the patient. A set of pads made of special foam was used to adjust the table height according to the patient size. The three triangulation lasers (centre and laterals) identical to those used on the linear accelerators were used for patient positioning.

2.2. MR geometrical distortions and the GDC software

In MR imaging, each point in the imaging space is associated with a resonance frequency, which is generated by the linear magnetic field gradient. In one dimension, say the x direction, this can be expressed by

$$\varpi(x) = \gamma(B_0 + xG_x) \quad (1)$$

where B_0 and G_x are the main magnetic field intensity and the magnetic field gradient in the x direction respectively, and γ is the gyromagnetic ratio. It is common knowledge that non-uniformity of B_0 and nonlinearity of G_x will introduce uncertainties to the images on the spatial localization of the different resonance frequencies because of the way MR images are reconstructed. These uncertainties were defined as MR imaging geometrical distortions.

MR imaging geometrical distortions can be divided into machine-induced geometrical distortion and patient-induced geometrical distortion (Michiels *et al* 1994). The machine-induced MR geometrical distortion includes the main field inhomogeneity, gradient field nonlinearity and eddy currents caused by the gradient switching. As has been demonstrated by many investigators (Michiels *et al* 1994, Chang *et al* 1990, Sumanaweera *et al* 1994, Schad *et al* 1987), the distortions induced by gradient nonlinearity and main magnetic field non-uniformity are stable and can be corrected independently of other machine induced distortions. The patient-induced geometrical distortions include susceptibility effects, chemical shift and flow, which generally cannot be corrected 'once and for all' because of its patient dependency. However, due to the high receiver bandwidth (>100 Hz/pixel) in the frequency encoding direction used in our routine scanning, and based on the fact that there are no patient-induced MR image artefacts detected with 0.2 T low magnetic field using receiver bandwidth >100 Hz/pixel in the frequency direction (Fransson *et al* 2001), the patient-induced geometrical distortion was considered negligible for our MR unit. Therefore, the machine-induced geometrical distortions to the images from our MR scanner can be detected, studied and corrected accurately.

A Federal Drug Administration (FDA) approved GDC software provided by the manufacturer was installed on our scanner for MR image post-processing. The effectiveness of the post-processing was evaluated using a standard phantom (F18 phantom) provided by the manufacturer (figure 1(b)). The F18 phantom is intended for evaluation of residual geometrical distortions in the images post-processed by the GDC software. The phantom consists of a rectangular grid of spherical markers in a single plane separated by 2.5 cm in both directions (17 columns and 15 rows). The phantom is 3 cm in thickness and supplied with a support structure that allows the F18 phantom to be fixed into a body/spine coil. The orientation of the marker plane can be selected to align with any of the fixed imaging planes. In our measurements, the F18 phantom was placed in the xy plane of the coordinate system (transverse plane) with $z = z_0$, x defined as horizontal and y as vertical.

It should be emphasized that MRI geometrical distortions are caused by non-uniformity of the magnetic field and gradient nonlinearity in the three-dimensional space. The residual distortions after the GDC are expected to be three-dimensional. Since MRI does not provide electron density information required for inhomogeneity corrections in dose calculation and, for some sites like the prostate, these corrections are not clinically significant (Photon Treatment Planning Collaborative Working Group 1991), we have used homogeneous geometry for both CT-based and MRI-based treatment planning. The homogeneous geometry makes the distortion correction in the inferior–superior direction unnecessary in dose calculation. The only corrections needed in MRI-based treatment planning are those in the transverse plane, which affect the patient external contours. In this study, only distortions in the transverse planes were considered.

The effective FOV after the GDC was established 36 cm within which the effect of residual MR distortions on patient external contours was less than 5 mm. A larger effective FOV is required for MRI-based treatment planning of patients with larger lateral dimensions. In this work we have quantified the residual distortions after the GDC in the areas outside the 36 cm FOV using the F18 phantom. A Synergy body/spine L coil was selected and the phantom (with the support structure) was inserted into the coil, guided by the laser beam. The coil was

placed at the centre of the 0.23T scanner with the phantom plane in the sagittal direction (the x and y plane of the coordinate system). The phantom was imaged at different positions with a small increment $\pm\Delta z$ in the z -direction. The images were then exported in the DICOM format and transferred to our development environment for processing. Since each marker's geometrical position on the phantom is known (also can be calculated accurately knowing the position of the centre of the phantom on the image), the distortions for the markers at different z positions can be quantified by comparison with the known geometrical positions of the markers. For each position along the z -direction, a mapping file, which records the distortions in the transverse plane, was derived based on the measurements of the markers, and a computer program was developed to correct the distortions point-by-point for any MR scans using the measured distortion maps stored in the files.

Since the F18 only has 17 markers in the horizontal direction and 15 in the vertical direction, the distortions outside the $40 \times 35 \text{ cm}^2$ central area were measured by shifting the phantom left and right a few centimetres to determine the effective FOV.

2.3. The point-by-point distortion correction method

Based on the distorted images of the grid points at different z positions, correction maps can be derived by comparisons of the distorted images with the physical pattern of the grid on the F18 phantom. These maps can then be applied to rectify patient images acquired at the corresponding positions, using identical imaging sequences and parameter settings.

To quantify the distortion, i.e. the differences between the corresponding marker points of the F18 phantom and the image acquired from the scanner, a Cartesian coordinate is introduced, and the origin $(0, 0)$ of the coordinate is set at the bottom left corner of the images. In the Cartesian coordinate, we define the distributions of the grid points as $\vec{r}_z^p(i, j)$ and $\vec{r}_z^s(i, j)$, where $\vec{r}_z^p(i, j)$ is the spatial distribution of the points on the F18 phantom and $\vec{r}_z^s(i, j)$ is the spatial distribution of the centres of the markers on the image scanned, respectively. The distortion maps can then be defined as

$$\vec{M}_z(i, j) = \vec{r}_z^p(i, j) - \vec{r}_z^s(i, j) \quad (2)$$

where $i = 1, 2, \dots, 17$ and $j = 1, 2, \dots, 15$.

Once the maps of the geometrical distortions of the markers are established, they can be used to correct the residual distortions of MR images.

Figure 2 demonstrates the principles of mapping the pixels within the area defined by four marker points on the F18 phantom and the corresponding area on the distorted images. We assumed that the mapping area on the distorted image is quadrilateral, which may introduce uncertainties in the distortion corrections since a quadrangle may not have a quadrilateral image due to gradient distortion and non-uniformity of the main magnetic field. However, the quadrilateral approach is a reasonable one since it will provide the required accuracy for our application.

Based on the quadrilateral approach, we can perform the point-by-point correction to the distorted images. First, those pixels inside the area defined by any four markers on the phantom image are correlated with these on the distorted image by a linear mapping. This is done by equally dividing the distance between any two points on both images and then correlating the areas defined by the connecting lines.

The area (distorted pixels) on the distorted image may be larger or smaller than the area (pixels) on the F18 phantom. Figure 3 shows a distorted pixel and its relationship with pixels on the distorted MR image. Assume that a pixel (m, n) on the F18 phantom has its corresponding distorted area on the MR image that is larger than the MR pixel size as shown

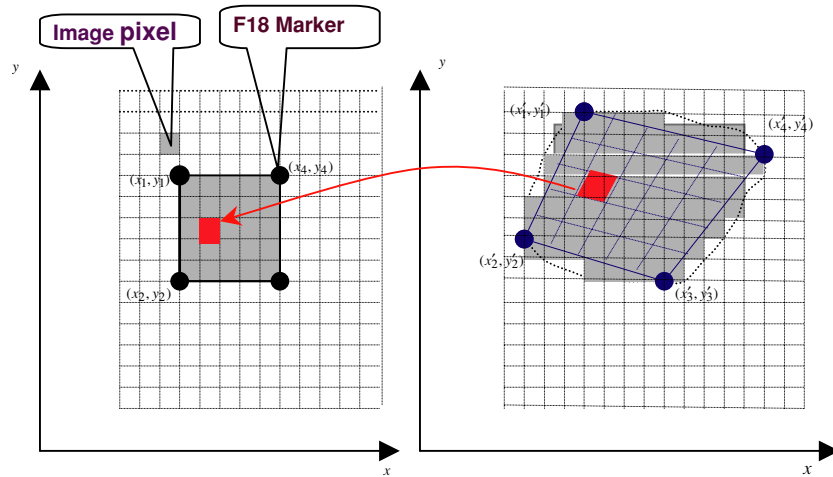


Figure 2. A diagram showing the mapping of the pixels between the distorted image and the F18 phantom.

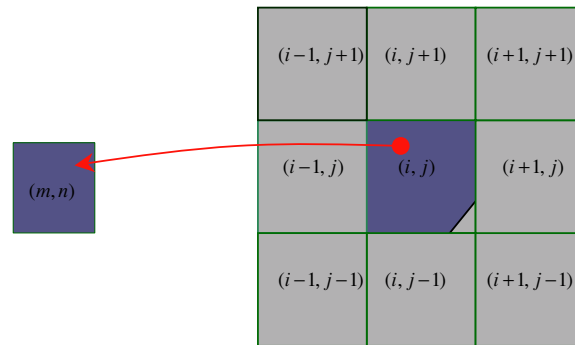


Figure 3. A diagram to illustrate the pixel intensity calculation.

in figure 3. The area covers not only the pixel (i, j) but also part of pixels $(i - 1, j)$, $(i, j - 1)$, $(i, j + 1)$, $(i + 1, j + 1)$ and $(i + 1, j)$. The overlapping areas here are represented by $\Delta(k, l)$ with $k = i - 1, i, i + 1$ and $l = j - 1, j, j + 1$. Then, the corrected intensity value for pixel (m, n) can be calculated as

$$I(m, n) = \frac{1}{S} \sum_{k,l} \Delta(k, l) \cdot I'(k, l) \quad (3)$$

where $k = i - 1, i, i + 1$ and $l = j - 1, j, j + 1$, S represents the value of the area (m, n) and $I'(k, l)$ is the image intensity for pixel (k, l) on the distorted MR image. If the distorted area of a pixel is smaller than the size of a pixel, the image intensity can be approximated by choosing $I(m, n) = I'(k, l)$.

2.4. Evaluation of the point-by-point distortion correction method

Since there is no patient-induced distortion for the 0.23 T MR unit with the sequences used in our study, the distortion maps derived from the phantom measurement can be used to correct

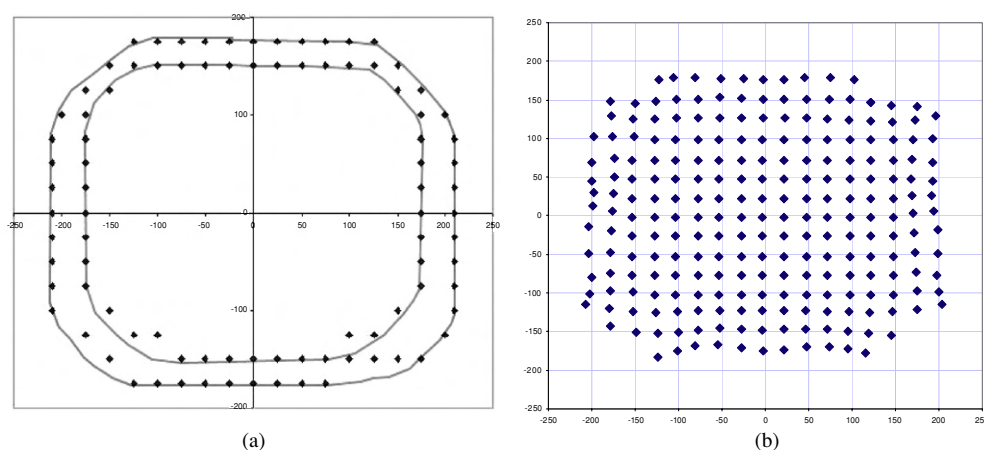


Figure 4. Actual viewable areas of the scanner and a distortion map. (a) The outer contour represents the viewable area of the transverse plane at the isocentre of the scanner and the inner contour the viewable area at the transverse planes 10 cm away from the isocentre plane along the I - S direction. The viewable areas for any transverse planes within 10 cm of the isocentre will be between the two contours. (b) A distortion map measured based on the F18 phantom measurement. Without distortion, any adjacent marker points laterally and vertically would have a 2.5 cm separation.

the residual MR distortions. However, detailed testing on real patients must be performed before its clinical implementation. In this work, distortion-free CT images were used to compare with MRI images of prostate patients before and after the GDC corrections.

It was understood that the differences between the CT and MRI external contours for the same patients resulted not only from MR image distortions but also from set-up uncertainties between CT and MR scans, which had to be minimized or excluded in order to evaluate the accuracy of the distortion correction. As previous investigators reported (Mah *et al* 2002, Chen *et al* 2005), the set-up uncertainties in CT and MR could be about 0.5 cm respectively. The combined set-up uncertainties in our CT and MRI comparisons were therefore expected to be ~ 0.7 cm (one standard deviation). Clinically, we have observed set-up uncertainties between CT and MR scans larger than 1 cm for some patients with large lateral dimensions.

In order to evaluate our point-by-point distortion correction method, static, porcine tissue samples were used in this study to eliminate the set-up uncertainties. We imaged frozen, porcine leg quarters on our CT and MRI scanners and arranged a pair of these to mimic human pelvis, using a special cradle to hold their positions firmly. All the MR images were scanned with our routine clinical three-dimensional fast spin echo sequences (3DFSE, 256×256 , 1.95 mm pixel, 3 mm slice thickness, TR = 3000 ms, TE = 140 ms, BW readout gradient > 100 Hz/pixel), and a standard FOV of 48 cm. The external contours from the CT images were exported to the MR images after fusion for direct comparison.

3. Results and discussion

Figure 4(a) shows the actual viewable areas of our 0.23 T MR unit for a standard 48 cm FOV for prostate imaging that indicate the geometrical limitations of the scanner at different transverse planes. The marker points outside the viewable areas were outside the 256 by 256 matrix due to the MR geometric distortions and were lost in the initial raw MR images. The

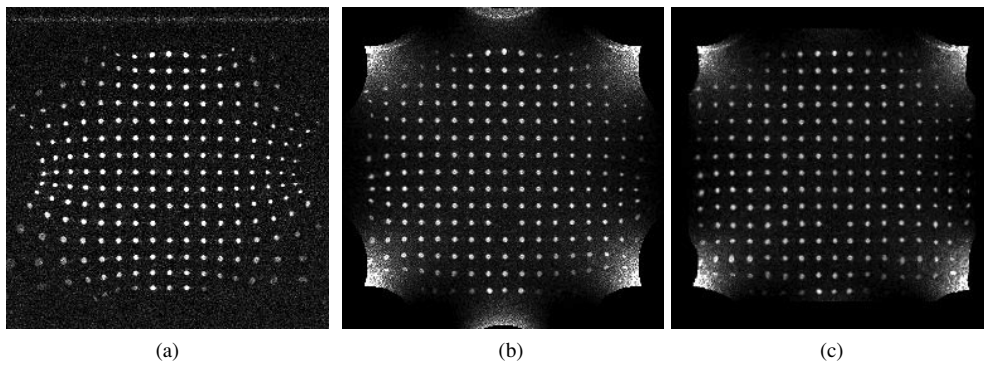


Figure 5. MR images of the F18 phantom at the isocentric plane: (a) before the GDC, (b) after the GDC, and (c) further corrected by the point-by-point distortion correction.

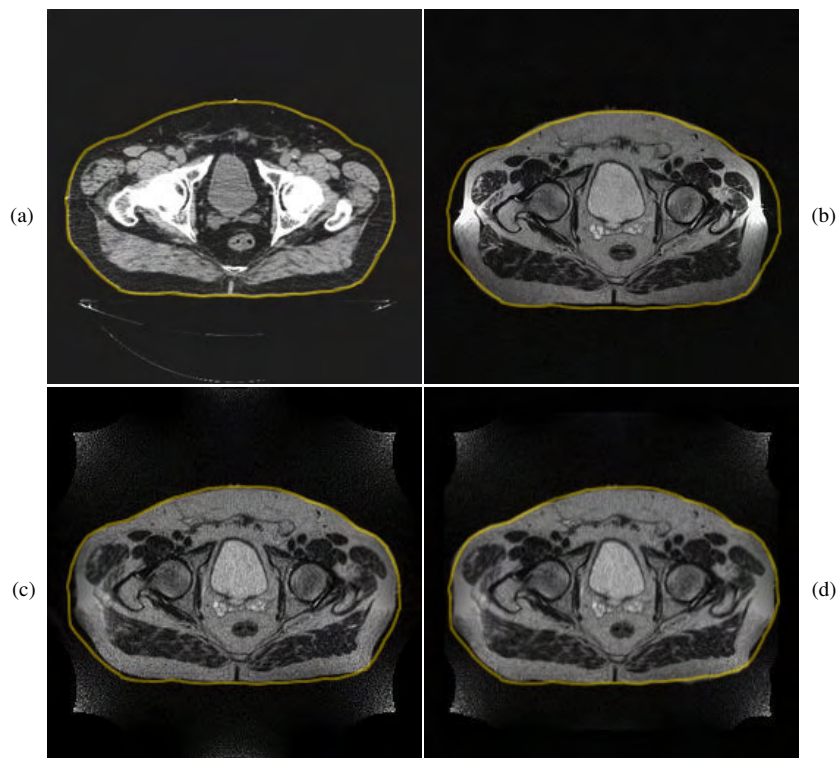


Figure 6. CT and MR images of a prostate patient: (a) a distortion-free CT image, (b) the same patient imaged on the MR scanner without any distortion corrections, (c) only with the GDC post-processing, and (d) with both the GDC and our point-by-point correction. The external contours on the MR images were exported from the CT image after image fusion.

GDC software reduced the MR geometric distortions significantly but could not recover the missing marker points. The outer contour in figure 4(a) represents the actual viewable area of the scanner at the isocentre transverse plane and the inner contour represents the actual viewable area which is 10 cm away from the isocentre. Any transverse planes within 10 cm

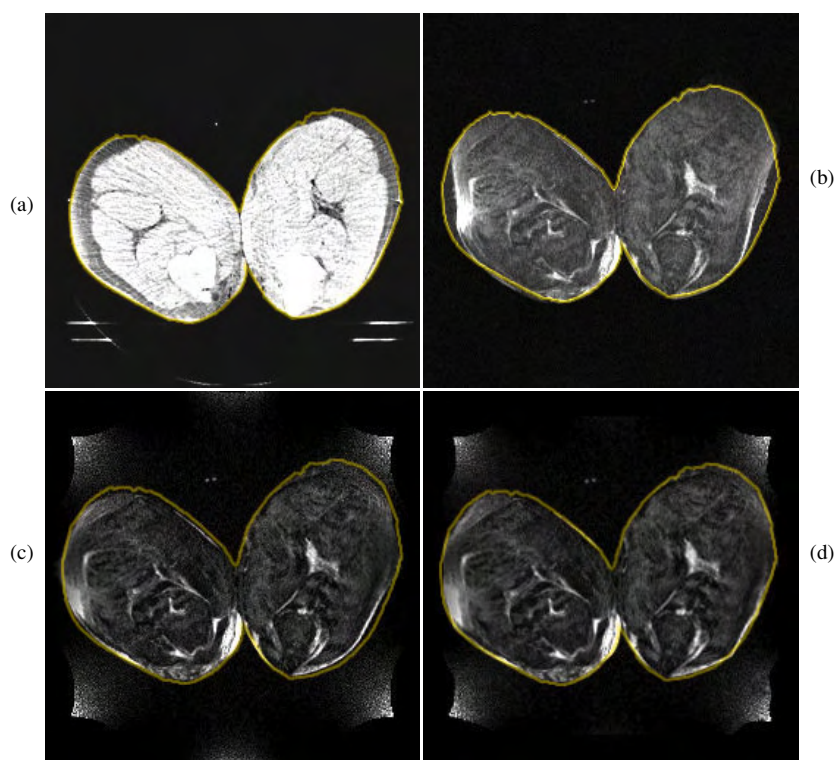


Figure 7. CT and MR images of frozen porcine samples: (a) a distortion-free CT image at the isocentric plane, (b) the same isocentric slice imaged on the MR scanner without any distortion corrections, (c) only with the GDC post-processing and (d) with both the GDC and our point-by-point correction. The external contours on the MR images were exported from the CT image after image fusion.

of the isocentre will have a viewable area between the two contours. The actual viewable area decreases with increasing distances from the isocentre, which is expected because of the loss of uniformity of the magnetic field at large distances. The distortion maps were established for every transverse plane along the I - S direction with a 0.5 cm interval and the maps were used to correct the distortions in our point-by-point distortion correction method. Figure 4(b) shows the distortion map of a transverse plane at the location of the scanner's centre. Compared with the physical pattern of the F18 phantom, the residual distortions after the GDC can be observed and the maximum distortion is about 1 cm.

Figure 5 shows MR images of the F18 phantom with and without the GDC post-processing and after the point-by-point corrections. These images were taken at the centre of the scanner with a standard FOV of 48 cm for prostate imaging. We then established a new effective FOV based on the viewable area for this transverse plane, which showed clinically insignificant distortions after the point-by-point correction. We established the effective FOVs for all the transverse planes in the same way. For later routine clinical applications, only the image points within the effective FOVs were processed. The maximum distortions were about 1.0 cm before the point-by-point correction and were reduced to <0.3 cm after the correction. The improvement on the marker positions is shown clearly.

A few patients were selected and processed to test our method. We found that the distortions were reduced dramatically after applying the GDC and our point-by-point

corrections. Figure 6 shows a distortion-free CT image with an external contour drawn by a physician and two MR images with and without the GDC and a MR image with both the GDC and the point-by-point distortion correction. The maximum residual error after our point-by-point distortion correction is expected to be ~ 0.3 cm based on the investigation results using the F18 phantom (up to 2 cm distortions were corrected compared with the initial image). From figure 6(d), the differences between the CT external contour and the distortion corrected image are still seen. It was believed that the major reason for these differences was the set-up uncertainty between the CT and MR scans.

To demonstrate this, we performed paired CT and MR scans for large, static porcine samples immobilized in a specially made cradle. Figure 7(a) shows a distortion-free CT image of the porcine samples, which were 42 cm in lateral dimensions. The external contour of the CT image was transferred to the MR images for comparison. The maximum distortion measured on the initial MR image was 2.1 cm (figure 7(b)) and significant residual distortions were still observable after the DGC post-processing (figure 7(c)). Measurements on the final MR image showed that the MR geometrical distortions were reduced to < 0.3 cm after our point-by-point distortion correction (figure 7(d)).

4. Conclusions

In this paper, we have described our work on MR image distortion correction to further improve the accuracy of dose calculation for MR-based treatment planning for prostate cancer. Our goal was to develop practical methods for the clinical implementation of MRI-based treatment planning. Our studies showed that, with our routine clinical three-dimensional fast spin echo sequences (3DFSE, 256×256 , 1.855 mm pixel, TR = 140 ms, TE = 3000 ms, BW readout gradient > 100 Hz/pixel), there were no patient-induced distortions. Therefore, the residual machine specific geometrical distortions after the GDC could be quantified by phantom measurements and further reduced by our point-by-point correction technique. The effective FOVs of the scanner were established based on the actual viewable areas with adequate geometric distortion corrections (ensuring < 5 mm distortion error). The effective FOV for prostate imaging using a standard FOV of 48 cm has been expanded from 36 cm using the existing GDC software to 42 cm using the point-by-point distortion correction technique developed in this work. Our results indicated that, with the distortion maps established in this work, we could correct MR geometrical distortions for patients of lateral dimensions up to 42 cm. Significant improvement in dose calculation has been achieved based on a 1–2 cm improvement in patient external contour determination.

Acknowledgments

The authors wish to thank their colleagues Dr R Price, Dr S Stathakis, Dr W Xiong and Dr J Fan for helpful discussions. They are also grateful to the support from Philips Medical Systems. The work was supported in part by grants from the DOD (PC030800) and the NIH (CA78331).

References

- Beavis A W, Gibbs P, Dealey R A and Whitton V J 1998 Radiotherapy treatment planning of brain tumours using MRI alone *Br J. Radiol.* **71** 544–8
- Chang H and Fitzpatrick J M 1990 Geometrical image transformation to compensate for MRI distortions *Proc. SPIE* **1233** 116–27

- Chen L *et al* 2005 Image guided radiation therapy: investigation of interfraction setup and external contour variation for prostate IMRT using CT and MRI *Abstract for 2005 AAPM Annual Meeting*
- Chen L, Li J, Mah D, Ma C M, Wang L, Ding M, Freedman G, Movsas B and Pollack A 2002 Monte Carlo investigation of dosimetry accuracy for MR-based treatment planning *Med. Phys.* **29** 1339 (abstract)
- Chen L *et al* 2003 Evaluation of MRI-based treatment planning for prostate cancer using a commercial TPS *Med. Phys.* **30** P1507
- Chen L *et al* 2004a MRI-based treatment planning for radiotherapy: dosimetric verification for prostate IMRT *Int. J. Radiat. Oncol. Biol. Phys.* **60** 636–47
- Chen L *et al* 2004b Dosimetric evaluation of MRI-based treatment planning for prostate cancer *Phys. Med. Biol.* **49** 5157–70
- Chen Z *et al* 2004c Investigation of CT-MR image intensity correlation for MRI-based dose calculation *Med. Phys.* **31** (abstract)
- Debois M, Oyen R, Maes F, Verswijvel G, Gatti G, Bosmans H, Feron M, Bellon E, Kutcher G, Van Poppel H and Vanuysel L 1999 The contribution of magnetic resonance imaging to the three-dimensional treatment planning of localized prostate cancer *Int. J. Radiat. Oncol. Biol. Phys.* **45** 857–65
- Fransson A, Andreo P and Potter R 2001 Aspects of MR image distortions in radiotherapy treatment planning *Strahlenther. Onkol.* **177** 59–73
- Guo W Y 1998 Application of MR in stereotactic radiosurgery *J. Magn. Reson. Imaging* **8** 415–20
- Hanks G E 1999 Progress in 3D conformal radiation treatment of prostate cancer *Acta Oncol.* **38** 69–74
- Hanks G E *et al* 1998 Dose escalation with 3D conformal treatment: five year outcomes, treatment optimization and future directions *Int. J. Radiat. Oncol. Biol. Phys.* **41** 501–10
- Khoo V S, Adams E J, Saran F, Bedford J L, Perks J R, Warrington A P and Brada M 1999 A comparison of MRI and CT for the radiotherapy planning of prostate cancer: a feasible study *Br. J. Radiol.* **72** 1309–17
- Kondziolka D, Dempsey P K, Lunsford L D, Kestle J R W, Dolan E J, Kanal E and Tasker R R 1992 A comparison between magnetic resonance imaging and computed tomography for stereotactic coordinate determination *Neurosurgery* **30** 402–7
- Lee Y K and Bollet M 2003 Radiation treatment planning of prostate cancer using magnetic resonance imaging alone *Radiother. Oncol.* **66** 203–16
- Mah D, Michael Hanlon S A, Freedman G, Milestone B, Mitra R, Shukla H, Movsas B, Horwitz E, Vaisanen P P and Hanks G E 2002 MRI Simulation: effect of gradient distortions on three-dimensional prostate cancer plans *Int. J. Radiat. Oncol. Biol. Phys.* **53** 757–65
- Michiels J, Bosmans H, Pelgrims P, Vandermeulen D, Gybels J, Marchal G and Suetens P 1994 On the problem of geometric distortion in magnetic resonance images for stereotactic neurosurgery *Magn. Reson. Imaging* **12** (5)
- Pollack A, Zagars G K and Rosen I I 1999 Prostate cancer treatment with radiotherapy: maturing methods that minimize morbidity *Semin. Oncol.* **26** 150–61
- Pollack A, Zagars G K, Smith L G, Lee J J, von Eschenbach A C, Antolak J A, Starkschall G and Rosen I 2000 Preliminary results of a randomized radiotherapy dose-escalation study comparing 70 Gy with 78 Gy for prostate cancer *J. Clin. Oncol.* **18** 3304–911
- Philips 2003 Radiation Therapy Support Kit, Instruction for use, Release 4.0.2
- Photon Treatment Planning Collaborative Working Group 1991 Role of inhomogeneity corrections in three-dimensional photon treatment planning *Int. J. Radiat. Oncol. Biol. Phys.* **21** 59–69
- Rasch C, Barillot I, Remeijer P, Touw A, van Herk M and Lebesque J V 1999 Definition of the prostate in CT and MRI: a multi-observer study *Int. J. Radiat. Oncol. Biol. Phys.* **43** 57–66
- Roach M 3rd, Faillace-Akazawa P, Malfatti C, Holland J and Hricak H 1996 Prostate volumes defined by magnetic resonance imaging and computerized topographic scans for three-dimensional conformal radiotherapy *Int. J. Radiat. Oncol. Biol. Phys.* **35** 1011–18
- Schad L R, Boesecke R, Schlegel, Gunther W, Hartmann H, Sturm V, Strauss L G and Lorenz W 1987 Three dimensional image correlation of CT, MR, and PET studies in radiotherapy treatment planning of brain tumors *J. Comput. Assist. Tomogr.* **11** 948–54
- Sumanaweera T, Glover G, Song S, Adler J and Napel S 1994 Quantifying MRI geometric distortion in tissue *Magn. Reson. Med.* **31** 40–7
- Zelevsky M J *et al* 1998 Dose escalation with three-dimensional conformal radiation therapy affects the outcome in prostate cancer *Int. J. Radiat. Oncol. Biol. Phys.* **41** 491–500

Monte Carlo dose verification of MR image based IMRT treatment planning for prostate cancer

Z. Chen, C-M Ma, J. Yang, J. Li, W. Luo, J. Fan, K. A. Paskalev, R. A. Price Jr, Y. Chen and L. Chen,
Department of Radiation Oncology, Fox Chase Cancer Center, Philadelphia, Pennsylvania, 19111
E-mail: chenz@karmanos.org

MR-based treatment planning for prostate IMRT has been successfully developed and implemented in our department. In a previous work, we have performed dose verification on a commercial treatment planning system (TPS) for the MR-based treatment planning. However, due to the limitation of our low field MR scanner (2 mm achievable resolution) and the inflexibility of image processing on the TPS, uncertainties were existed in the comparisons of the CT and the MR-based plans. Our previous work also showed the discrepancies in dose calculations in IMRT planning between using Monte Carlo method and the TPS with non-coplanar beam arrangements that a large amount of bones in pelvic area were irradiated. In this work, we used the Monte Carlo to further verify the dosimetric accuracy and consistency for the MR-based IMRT treatment planning and to study the inhomogeneity effect by using bulk density assignments to bony structures on MR images. Fifteen prostate patients were studied using homogeneous geometry based on CT and MRI, and heterogeneous geometry built based on CT numbers or different bulk densities for MR bony structures. For IMRT treatments with coplanar beam arrangements, the mean dose values of the CTV for homogeneous geometry based on CT were about 2% higher than those for heterogeneous geometry based on CT. The difference in the mean CTV dose between homogenous MRI and heterogeneous CT geometries was about 3% and less. The DVH curves also agreed to within 5% in dose or volume among these plans. For treatments with larger discrepancies found in the CTV dose between homogeneous and heterogeneous geometry due to the attenuation of the oblique beams going through the femurs, bulk-density assignment to femurs and femoral heads were used and a 1.8g/cm³ optimal bulk-density was found to reduced the discrepancies from 10% to less than 3% in MR-based planning.

I. Introduction

Since the past a couple of years, a sophisticated technique and a practical procedure have been developed and implemented clinically in our department for MR-based treatment planning for prostate cancer.⁽¹⁾ We have developed an efficient method to quantify and correct the machine induced geometrical distortions to less than 0.3 cm.⁽²⁾ We have performed dose verification for MR-based treatment planning on a commercial treatment planning system (TPS) and good agreements were achieved between CT and MR-based dose calculations.⁽¹⁾ However, due to the limitation of our low field MR scanner (2 mm achievable resolution) and the inflexibility of image processing on the TPS, some discrepancies were found in our previous work during the comparisons of the CT and the MR-based plans, especially for the doses to the critical structures, such as doses to rectum and bladder. Discrepancies in dose calculations of IMRT planning were also existed between using Monte Carlo method and the TPS with non-coplanar beam arrangements that a large amount of bones in pelvic area were irradiated.⁽³⁾ In this work, we use the Monte Carlo method to perform dose calculation to: 1) further verify the accuracy and consistency of the dose calculation in the MR-based treatment planning; 2) investigate the inhomogeneity effect in the CT-based calculation and to compare the CT results with bulk-density assignment in MR-based calculations.

II. Materials and methods

A. IMRT planning

The images for all the patients in this work were acquired on a Picker AcQSim CT scanner and a Philips MR 0.23 T open scanner (Philips Medical System, Cleveland, OH). Target and critical structures were delineated by the physicians based on the fused CT and MR images using the AcQSim VoxelQ segmentation tools. The IMRT plans were generated on the Corvus inverse-planning system (Version 5) based on the CT data (Nomos Corp. Sewickley, PA). Once the plan was approved by the physician, it was moved to our Monte Carlo system with the patient's CT and contour data, treatment isocenter, leaf-sequencing files and beam parameters for dose calculation. On the Monte Carlo treatment planning system, images were further processed so that the FOV, voxel size and volumes of RT structures were kept the same for both CT-based and MR-based dose calculations.

B. Monte Carlo dose calculation

The Monte Carlo code used in this work for dose calculation was MCSIM, which is an EGS4/PRESTA user code developed at Fox chase Cancer Center (FCCC).^(4,5) The beam information was represented using a source model, which was built based on measured beam data^(8,7,6), and validated for Monte Carlo dose calculation for photon beams from our Siemens accelerators. During the calculation, the multi-leaf collimator leakage effect was taken into account when intensity maps were reconstructed

Monte Carlo dose verification of MR image based IMRT treatment planning for prostate cancer

from a plan. The accuracy of the dose calculation is better than 2% compared with measured data.^{9,10} For each patient, an RTP file from the Corvus treatment planning system that includes patient setup parameters and beam and leaf-sequence information was used for the Monte Carlo simulation. The electron and photon energy cutoffs, ECUT and PCUT, for particle transport in the Monte Carlo simulations were set to 700 keV and 10 keV, respectively. The energy thresholds for δ ray production (AE) and for Bremsstrahlung production (AP) were also set to 700 keV and 10 keV, respectively. The maximum fractional energy loss per electron step (ESTEP) was set to 0.04 and the default parameters were used for the PRESTA algorithm. Seventy million particle histories were used to achieve less than 0.5% statistical uncertainties to the target dose for all the IMRT plans. Each photon was split 20 times to improve the simulation efficiency using the photon-splitting technique implemented in MCSIM.

C. Investigation of inhomogeneity effect for MR-based calculation

CT-based IMRT Monte Carlo dose calculations with and without heterogeneity correction were performed for each selected plan in order to investigate heterogeneity effect caused by different beam angle arrangements. Based on the results, MR-based IMRT dose calculations were then performed to the plan using either uniform density geometry or uniform density geometry with bulk electron density assigned to bony structures. For the plans with insignificant inhomogeneity effect, uniform geometries with water density were used in the MR-based dose calculation. For the plans that bony structure constitutes a large part of volume irradiated, uniform density geometry with bulk electron density assigned to bony structures was used in the MR-based dose calculation.

D. Dose verification of MR-based plan

The differences in isodose distributions and dose-volume histograms (DVH) were used to compare the results of the CT-based and the MR-based dose calculations for each IMRT plan. The clinical quantities such as target volume (CTV), the mean dose, maximum and minimum dose received by the CTV and the critical structures were chosen for the comparison. The maximum dose was defined as the highest dose received by 1% of the target volume and the minimum dose was defined as the lowest dose received by 99% of the target volume, respectively. The paired CT and MR data for any patients in this work were pre-processed to have the same pixel resolution. A special computer code was developed to convert the patient CT and MR image data from the DICOM format to geometries specially formatted for the MCSIM code.

III. Results and discussions

With proper geometrical distortion corrections for the MR images and the use of uniform water equivalent density geometry in the dose calculations, it was expected that the IMRT plans based on CT and MR data would agree well. Figure 1 shows the DVH curves from the CT and MR-based dose calculations for one of the 10 IMRT plans investigated. This IMRT plan used 10 MV photon beams with 9 gantry angles on a Siemens Primus accelerator with 39 fractions to deliver 78 Gy. The difference in the mean dose of the CTV was 0.3% between the CT-based and MR-based calculations. The differences in the maximum dose and in the minimum dose of the CTV were 0.8% and 0.2% respectively. Figure 2 shows the isodose distributions from the CT- and MR-based calculations for this patient.

Table 1 lists the differences of the clinical quantities in the dose calculations using MR data and CT data with homogeneous water equivalent geometries for 10 IMRT prostate plans with co-planar beam arrangements, as well as the differences of the clinical quantities between MR-based dose calculations with uniform water equivalent geometry and CT-based dose calculations with heterogeneity corrections. The data presented in Table 1 were calculated as the percentage differences between CT-based and MR-based results, i.e., $(D_{CT} - D_{MR})/D_{MR} \times 100\%$, where D_{CT} is the dose from CT-based calculation and D_{MR} is the dose predicted by MR-based calculation. ΔD_{min} is the difference in the minimum dose of the target, ΔD_{mean} is the difference in the averaged target dose, ΔD_{max} is the difference in the maximum target dose, and ΔD_5 and ΔD_{95} are the differences of the dose received by 5% and 95% of the target volume, respectively. Table 1 also shows, with the co-planar beam arrangements, the averaged differences using MR data with uniform water equivalent geometries and CT data with heterogeneity corrections for all the clinical quantities used in this comparison were less than 2% , and the maximum differences were also less than 4% and the averaged differences over the 10 IMRT plans were less than 1.6% for all the quantities in the comparison, indicating that the uniform geometry was a good approach with our commonly used beam arrangements.

For some clinical cases non-coplanar beam arrangements where a large amount of pelvic bones were irradiated in the treatment, heterogeneity correction became necessary in planning. More than 8% differences in dose calculations were observed in the comparisons of DVHs for some CT-based IMRT plans with and without heterogeneity correction. To utilize MR-based planning for the treatments with large amount of pelvic bones irradiated, inhomogeneity corrections must be taking into account and bulk-density assignment to bony structures was proposed since there is no simple point-to-point correlation between MR signal intensities and electron densities of the materials imaged^{11}. Various bulk-density assignments to the femurs and femoral heads were studied in this work. Figure 3 shows the changes in the DVH with different bulk density

Monte Carlo dose verification of MR image based IMRT treatment planning for prostate cancer

assigned to the femurs (between 1.5 and 2.2 g/cm³) for two IMRT plans with large amount of pelvic bones irradiated. Table 2 shows the target doses based on CT data with heterogeneity correction and based on MR data with and without bulk densities assigned to the femurs and femoral heads for a 7-field IMRT plan with 7-field non-coplanar beams. The averaged target doses for each beam as calculated using CT data with heterogeneous correction and using MR data with bulk-density assignment agreed well compared with CT uniform water equivalent geometry. For those beams with gantry/table angles as 275/340, 85/20 and 85/0, the differences in the average target doses were decreased from about 10% with uniform water equivalent geometry to about 3% or less after using 1.8g/cm³ bulk density assignment to femurs and femoral heads. The changes in DVHs using CT data with 1.8g/cm³ bulk density for the femurs and femoral heads also confirmed our findings.

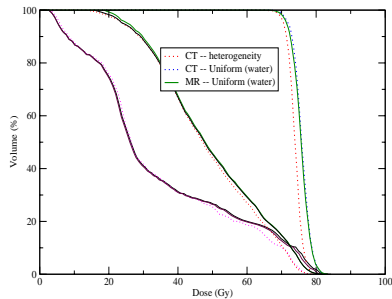


Figure 1. Comparison of the DVHs for a co-planar plan calculated based on CT data with and without heterogeneity correction and based on MR data in uniform geometry (1 g/cm³).

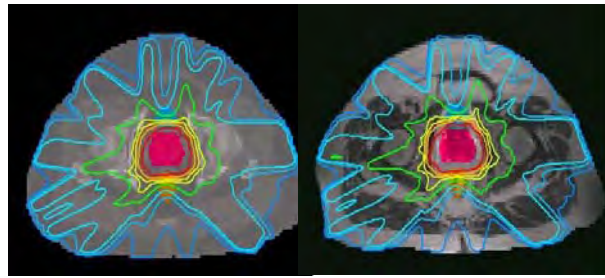


Figure 2. Isodose comparison between CT-based dose calculation without heterogeneity correction and MR-based dose calculation in uniform geometry (1 g/cm³).

The values of 1.8g/cm³ for optimal bulk-density assignment for the femurs and femoral heads were obtained based on the results of our calculations only. We have used different bulk-density assignments in the dose calculations for IMRT plans, 4 beam conformal plans and single beams with different incident angles and compared the results with those predicted by CT data with heterogeneity corrections; 1.8g/cm³ gave the best fit.

For critical organs in prostate treatment, such as rectum and bladder, the dose differences between CT- and MR-based calculations were negligible compared with the differences in the target dose for all the plans studied (see figures 1 and 3). The results

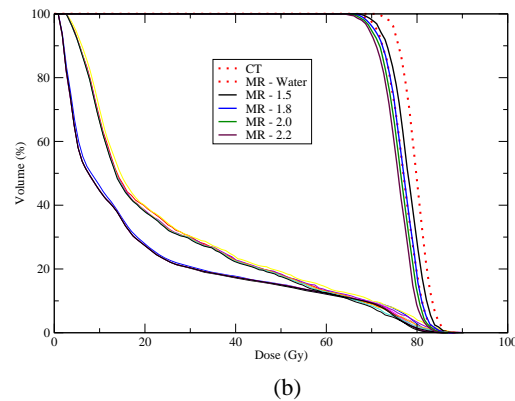
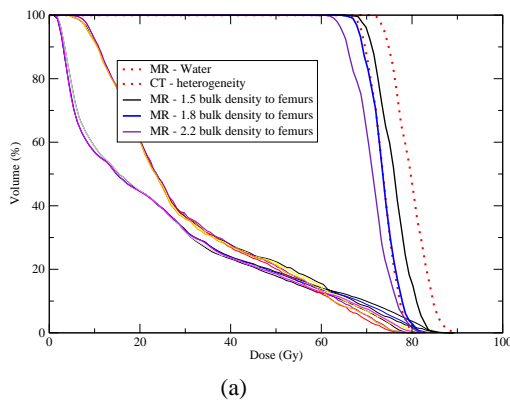


Figure 3. Comparison of DVHs for non-coplanar plans between CT-based dose calculation with heterogeneity correction and MR-based dose calculation. Different bulk densities were assigned to the femurs in MR-based dose calculations. a) a 7 beam plan with table angles at 25⁰, 20⁰, 0⁰, 0⁰, 0⁰, 340⁰, and 330⁰; and b) a 9 beam plan with table angle at 25⁰, 20⁰, 0⁰, 0⁰, 0⁰, 0⁰, 0⁰, 340⁰ and 335⁰.

Table 1 Target dose differences between CT-based and MR-based treatment plans. The values at the left in the brackets are the differences in target doses calculated based on MR and CT with water equivalent uniform geometry; the values at the right in the brackets are the differences in target doses calculated based on MR with water equivalent uniform geometry and CT with heterogeneity correction for 10 IMRT plans of prostate cancer patients

Patient	$\Delta D_{mean}(\%)$	$\Delta D_{min}(\%)$	$\Delta D_{max}(\%)$	$\Delta D_5(\%)$	$\Delta D_{95}(\%)$
1	(0.1 , 1.3)	(1.5 , 1.6)	(1.2 , 1.0)	(1.0 , 1.3)	(0.4 , 1.7)
2	(2.1 , 0.5)	(2.7 , 0.5)	(1.7 , 2.1)	(2.3 , 1.0)	(0.5 , 0.5)
3	(1.6 , 1.5)	(0.4 , 1.4)	(2.5 , 0.6)	(2.6 , 0.8)	(0.8 , 1.6)
4	(0.8 , 0.9)	(3.1 , 0.3)	(0.9 , 0.3)	(0.4 , 1.2)	(2.1 , 0.9)
5	(1.0 , 1.5)	(0.2 , 1.4)	(1.6 , 1.0)	(1.4 , 1.7)	(0.5 , 1.6)
6	(1.7 , 2.6)	(0.2 , 3.2)	(2.9 , 1.7)	(2.7 , 2.7)	(0.7 , 2.7)
7	(0.3 , 2.7)	(0.8 , 1.7)	(0.2 , 3.5)	(0.2 , 3.2)	(1.2 , 1.9)
8	(1.2 , 1.3)	(1.2 , 1.2)	(1.9 , 0.7)	(1.5 , 0.9)	(0.6 , 1.4)
9	(0.5 , 2.3)	(0.7 , 2.6)	(0.5 , 2.0)	(0.5 , 2.1)	(0.5 , 2.5)
10	(0.1 , 1.5)	(0.1 , 1.9)	(0.2 , 1.3)	(0.1 , 1.1)	(0.2 , 1.4)
Average	(0.9 , 1.6)	(1.1 , 1.6)	(1.4 , 1.4)	(1.3 , 1.6)	(1.0 , 1.6)

Table 2 Differences in the target dose with and without heterogeneity correction and with bulk density assignment for a 7-field, non-coplanar IMRT plan. $\Delta_1\%$ represent the percentage differences with and without heterogeneity correction; $\Delta_2\%$ represent the percentage differences with heterogeneity correction and 1.8 g/cm bulk density assigned to femurs and femoral heads.

Beam	Gantry	Couch	Ave. target dose cGy	Ave. target dose (w) cGy	Ave. target dose (1.8)	$\Delta_1\%$	$\Delta_2\%$
1	0	0	45.4	47.0	46.2	3.40	1.7
2	275	0	20.5	22.4	19.7	8.48	4.1
3	275	340	19.8	22.2	19.9	10.81	0.5
4	280	25	38.2	40.9	38.0	6.60	0.5
5	85	20	21.6	24	21.9	10.00	1.4
6	85	0	20.7	23.1	20.0	10.39	3.5
7	85	330	38	41.4	38.8	8.21	2.1
Sum			204.2	221.0	204.5	8.27	2.0

IV. Conclusion

We found that the differences in the results between CT data (with heterogeneity correction) and MR data (with uniform water equivalent geometry) were about 3% or less and less than 2% in the mean values for the 10 plans with beams arranged in one axial plane (see table 1). For MR-based calculations (with homogeneous geometry), our results demonstrated that the differences between MR-based calculations and CT-based calculations (without heterogeneity correction) were less than 2% for the individual patients and about 1% in the mean values, which proved that MR-based IMRT plans can be used to replace CT-based planning clinically (see table 1). The 1% - 2% differences in dose calculations were mainly caused by the setup uncertainties of the two imaging modalities if geometrical distortions on the MR images were corrected to less than 3 mm.

For treatments in which relatively large amount of bones are irradiated, MR-based treatment planning with homogeneous geometry would not be appropriate because of the excessive attenuation of the photon beams passing through bony structures. However, by assigning bulk densities to the bony structures especially for the femurs and femoral heads, the dose differences could be reduced to less than 3% (see table 2). The bulk densities assigned to the femurs that gave the best fits to CT-based calculations with heterogeneity correction were 1.8g/cm³ in our simulations.

We have established a practical procedure for MR-based treatment planning, in which MR geometrical distortions are properly corrected, a useful DRR technique⁽¹⁾ is developed/implemented and homogeneous geometry is used in the dose calculation. Our results show that it is accurate and consistent in dose calculation for prostate cancer treatment. In our department, one third of radiotherapy treatments are for prostate cancer and homogeneous geometry has been used in prostate planning dose calculation. By using MR-based treatment planning the savings in staff time, patient time and treatment costs would be significant and the additional radiation exposure from CT scans can be avoided. It is concluded that MR-based radiotherapy treatment planning can be widely utilized clinically for prostate cancer treatment. Further investigations are carried out for other sites where heterogeneity effect is not significant.

Acknowledgements

The authors wish to thank Dr. S. Stathakis, Dr. William Xiong their helpful discussion. The work is supported in part by grants from the DOD (PC030800) and the NIH (CA78331).

References

1. Chen L, Price R, Nguyen T-B, Wang L, J S Li, Qin L, Ding M, Palacio E, Ma C-M and Pollack A Dosimetric evaluation of MRI-based treatment planning for prostate cancer Phys. Med. Biol. 2004; 49: 5157-5170
2. Z Chen, C-M Ma, K Paskalev, J Li, J Yang, T Richardson, L Palacio, X Xu and L Chen, Investigation of MR image distortion for radiotherapy, Phys. Med. Biol. 2006; 51: 1393-1403
3. Yang J, Li J S, Chen L, Price R, McNeeley S, Qin L, Wang L, W Xiong and Ma C-M Dosimetric verification of IMRT treatment planning using Monte Carlo simulations for prostate cancer Phys. Med. Biol. 2005; 50: 1-10.
4. Ma C-M, Li J S, Pawlicki T, Jiang S B, Deng J, Lee M C, Koumrian T, Luxton M and Brain S A Monte Carlo dose calculation tool for radiotherapy treatment planning Phys. Med. Biol. 2002; 47: 1671-89
5. Ma C-M, Pawlicki T, Jiang S B, Li J S, Deng J, Mok E, Kapur A, Xing Lei, Ma L and Boyer A L Monte Carlo verification of IMRT dose distributions from a commercial treatment planning optimization system Phys. Med. Biol. 2002; 45:2483-95.
6. Jiang S B, Boyer A L, and Ma C-M Modeling the extrafocal radiation and monitor chamber backscatter for photon beam dose calculation Med. Phys. 2001; 28:55-66
7. Jiang S B, Deng J, Li J S, Pawlicki T, Boyer A L, and Ma C-M Modeling and commissioning of clinical photon beams for Monte Carlo treatment planning XIII ICCR 2000 ed W Schlegel and T Bortfeld pp 434-6
8. Yang J, Li J S, Qin L, Xiong W and Ma C-M Modeling of electron contamination in clinical photon beams for Monte Carlo dose calculation Phys. Med. Biol. 2004; 49:2657-73
9. Li J S, Pawlicki T, Deng J, Jiang S B and Ma C-M Validation of a Monte Carlo dose calculation tool for radiotherapy treatment planning Phys. Med. Biol. 2000; 45:2969-85
10. Ma C-M, Mok E, Kapur A, Pawlicki T, Findley D, Brain D S, Forster K, and A. L. Boyer A L Clinical implementation of a Monte Carlo treatment planning system Med. Phys. 1999; 26:2133-43
11. Lee YK and Bollet M, Radiation Treatment Planning of Prostate Cancer Using Magnetic Resonance Imaging Alone, Radiotherapy and Oncology 2003; 66:203-216